UNIVERSIDADE TECNOLÓGICA FEDERAL DO PARANÁ – UTFPR
DEPARTAMENTO ACADÊMICO DE INFORMÁTICA
CURSO DE BACHARELADO EM ENGENHARIA DE COMPUTAÇÃO

GUSTAVO AKIRA GONDO

A QUARTZ CRYSTAL MICROBALANCE ELECTROCHEMICAL SENSOR-BASED CONTAMINATION DETECTION SYSTEM

TRABALHO DE CONCLUSÃO DE CURSO

CURITIBA

2021

GUSTAVO AKIRA GONDO

A QUARTZ CRYSTAL MICROBALANCE ELECTROCHEMICAL SENSOR-BASED CONTAMINATION DETECTION SYSTEM

Trabalho de Conclusão de Curso apresentado ao Departamento Acadêmico de Eletrônica e ao Departamento Acadêmico de Informática da Universidade Tecnológica Federal do Paraná como requisito para a obtenção do grau de "Bacharel em Engenharia de Computação" da Universidade Tecnológica Federal do Paraná (UTFPR)

Orientador: Rubens Alexandre de Faria
Universidade Tecnológica Federal do Paraná

CURITIBA
2021

GUSTAVO AKIRA GONDO

TÍTULO DO TRABALHO: A QUARTZ CRYSTAL MICROBALANCE ELECTROCHEMICAL SENSOR-BASED CONTAMINATION DETECTION SYSTEM

Trabalho de Conclusão de Curso de Graduação apresentado como requisito para obtenção do título de Bacharel em Engenharia de Computação da Universidade Tecnológica Federal do Paraná (UTFPR).

Data de aprovação: 05/novembro/2021

_____

Wilson José da Silva
Titulação: Doutor
Universidade Tecnológica Federal do Paraná

_____

Leyza Baldo Dorini
Titulação: Doutora
Universidade Tecnológica Federal do Paraná

_____

Anderson Emanuel Ximim Gavim
Titulação: Mestre
Faculdades da indústria do Sistema FIEP

CURITIBA

2021

Abstract

Like many technological inventions of its kind, Quartz Crystal Microbalances (QCMs) have been applied to various different fields, from explosive detections to alcohol vapors classification. One field it has seldom seen use is in the detection of contaminants in aqueous environments, and in addition, few fully-formed contamination detection systems have been fully developed for the QCM platform. Therefore this work aims to develop a novel aqueous ammonia detection system along with the complete set of auxiliary systems for its operation, such as a graphical user interface and email notifications. The sensor film that coated the QCM was a polyaniline(PANI)/Reduced Graphene Oxide(rGO) composite that, when testing with the QCM system, achieved a range of $1mg/L$ to $100mg/L$ with an R^2 value of 0.9633, with a response time ranging from $290s$ to $25s$, being comparable in response time and sensitivity to other sensors. Paving way to a novel class of usages of electrochemical sensors and resonant piezoelectric crystals.

Key-words: Aqueous Ammonia, Electrochemical Sensor, PANI, QCM, QCM-R.

Acknowledgments

I would like to firstly thank my family and friends for their love and support during the troubled times this project was implemented in; My friends Olivia, Fernanda, Amanda, Thais, Paula, Sofia, Manami, Gabi, and Gabi C. I thank you immensely for being the great forces that allowed me to outperform what I expected of myself, and for that, I am forever grateful for you being the people that you are and for the friendship we have built. Thank you;

Professor Rubens Alexandre de Faria for being my advisor in this project, for the guidance you have given me, for allowing me to be more ambitious than I thought I could be, and for the opportunity to be able to work with you;

Professor Anderson Gavin for helping me countless times in everything that went outside of my understanding of chemistry and physics during the development of this project;

Professor Elder Oroski for the help in relation to the algorithms to be used in this project, and for your unwavering support during the implementation of this project;

Professor Wilson da Silva for allowing me to use your facilities for our experiments and your suggestions for improvements in this project;

Professor Jefferson de Deus for the synthesis of the reduced graphene oxide used in this project;

Professor Jefferson de Deus for the synthesis of the reduced graphene oxide used in this project;

The Multi-User Material Characterization Center (CMCM) at UTFPR for allowing us the usage of your facilities for the profilometry;

List of Figures

List of Tables

List of abbreviations and acronyms

DAINF	*Departamento Acadêmico de Informática*
DAELN	*Departamento Acadêmico de Eletrônica*
PANI	Polyaniline
rGO	Reduced Graphene Oxide
GUI	Graphical User Interface
LOD	Limit of Detection
TAN	Total Ammonia Nitrogen
KNN	K-Nearest Neighbors
QCM	Quartz Crystal Microbalance
LOF	Local Outlier Factor
COF	Connectivity Outlier Factor
HTM	Hierarchical Temporal Memory
PCA	Principal Component Analysis
CBLOF	Cluster Based Local Outlier Factor
OCSVM	One Class Support Vector Machine
SVM	Support Vector Machine

List of symbols

α	Greek symbol for alpha
β	Greek symbol for beta
γ	Greek symbol for gamma
Δ	Greek symbol for Delta
ρ	Greek symbol for Rho
η	Greek symbol for eta
μ	Greek symbol for mu
π	Greek symbol for pi

Summary

1 Introduction

The number of data capturing systems have grown exponentially throughout the previous years, from applications such as systems integrity monitoring, to industrial quality control, garnering a large amount of interest from a diverse number of industries in the development of novel types of sensors and sensor systems (HADANO et al., 2021)(LI et al., 2020). One such application that is vital for many of society's needs is in the constant quality control and contamination detection of drinkable water or water that is present in streams and rivers that have pollution-sensitive species such as a variety of species of mollusks and crustaceans (HUFF et al., 2013). An example of such pollution that is one of the most prevalent is ammonia, being extremely toxic in high concentrations to a few species of fish and mollusks and a strong indicator of other pollutants, its early detection in drinkable water is a vital component of its quality control (HUFF et al., 2013).

In this context, Quartz Crystal Microbalances (QCMs) have amassed interest from the scientific community by providing a novel, simple way of implementing a variety of types of sensors, such as antigen-based virus sensors (LIU; ZHANG, 2013), electrochemical explosive detectors (ESLAMI; ALIZADEH, 2019) and a variety of drug and contamination detectors (SONG et al., 2017). In addition, a large set of novel ammonia-sensitive films have been developed over the past decade, showing consistent improvements over previous sensors (LI et al., 2020). An example of such a sensor is a Polyaniline (PANI) and Reduced Graphene Oxide (rGO) composite film, which has been validated with the work presented in (HADANO et al., 2021), showing a great improvement in gaseous ammonia sensing.

The aim of this work is to combine all of these concepts in the usage of this novel PANI/rGO composite film within a QCM based sensor system in order to develop a real-time ammonia-contamination detection system.

1.1 Problem and Premises

The problem at hand is the detection of ammonia in water, one important distinction to be made is that this is a detection problem, as opposed to a classification or quantification problem, therefore, the main problem to be solved is to detect, above a certain concentration threshold, the presence of ammonia within a certain controlled water sample, meanwhile, questions as to which contaminant is present in the water and how much of that contaminant there is in the water, are not the main focus of this work, limitations of which are partially imposed by the inherent characteristics of QCM systems, as will be further described in Section 3.1.2.

The structure of this problem can be divided into two main parts: (i) the sensing of ammonia and (ii) its detection within a certain water sample. The sensing (i) pertains to the

development of the sensitive film and QCM systems in combination, as well as a study of how they behave together, characteristics and limitations. The detection (ii) applies to the back-end system that uses the readings provided by the QCM system in order to detect whether or not there has been a contamination or not within a given control sample and to signal, both the user and the system that that event has occurred.

In order to restrict the scope of this work, a few premises must be put in place:

- **There are no contaminants at time** $t = 0$: This simplifies the scope of the system by implying there is a control substance, whose readings can be used as a comparison in order to detect the contamination. The reason why this premise must exist for a QCM system is further exemplified in Section 3.1.2;
- **A Contamination below a given threshold range can be ignored**: This means that the contamination must be above the threshold defined in this work in order for it to be defined as a true contaminant.
- **The contamination happens in normal controlled conditions**: The environmental conditions will affect a measurement directly in a variety of different manners, the most notable of which are the effects of temperature, therefore, this work will restrict its environmental conditions to a temperature-controlled room at around 22^oC.

1.2 Objectives

1.2.1 General Objectives

To implement a continuous real-time contamination detection system utilizing Quartz Crystal Microbalance Sensors.

1.2.2 Specific Objectives

- **To develop an experimental setup for QCM measurements of different substances**: In order to develop the system, there must be a consistent and repeatable experimental setup in place so that the tests and experiments can be validated;
- **To define control measures in order to validate the experiment**: The implementation of this setup needs to take into account that any contaminants above a certain threshold need to be detects, that threshold needs to be duly justified through quantitative data;
- **To identify the best detection method of contaminations**: In order to optimize the performance of the system, a prior study of some detection methods must be performed based on what is known from the data;

- **To develop a detection model for the contaminants**: Based on what was seen in the analysis of detection methods, to develop a detection model based on the data collected from the QCM;
- **To test and evaluate the contamination detection model**: To test the model and evaluate its performance and whether or not it is a valid model. In case it isn't, it must be adapted in order to fit its goals based on the control measures.

1.3 Methodological Procedures

This work was divided into 4 distinct phases: the initial study of the problem, the design of the solution, the development/implementation of the system and the tests and evaluation/results of the sensor and detection system.

The study of the problem starts with the familiarization with the QCM based on prior research and documentation written on it, which provides a body of knowledge of its advantages and limitations and the necessary basis on which the system needs to be designed on. In this phase, the control measures will be brought up to be used as performance markers later on the project.

Based on that, the design of the solution will be created through the architecture of the system, the synthesis and test of the polymer coating and choosing the detection algorithms.

In the development and test phase, the system will be continuously tested and developed on in order to fit the necessary requirements set in the design phase of the project.

1.4 Structure of this Document

This document is organized in the following manner: Chapter 2 analyses related works in the field of electrochemical sensors, QCM-based gaseous ammonia sensors and other contamination detection systems that utilize electrochemical films for their sensing mechanism.

Chapter 3 explains how the theoretical foundation of how the QCM coated PANI/rGO sensor works, some of their advantages over other sensors, and their limitations. While Chapter 4 specifies the requirements that the system will have to undertake and some of their corollary functional requirements.

In Chapter 5.2, the development of the system and some preliminary results are shown and the, along with the architecture of the system and the models implemented for further testing in Chapter 6. Chapter 6 discusses the results obtained through the tests performed with the setup developed in Chapter 5.2, and finishes the implementation of the contamination detection system based on the results with the dataset collected from the experiments.

And in Chapter 7, discusses the results obtained and remarks about possible future works to be done as a consequence of this work.

2 State of the art and Related Works

2.1 Scope of the search

Due to the novelty of this work, there is amount of related works that tackle using QCMs in the detection of ammonia in aqueous environments, therefore, in this review of the state of the art, a broader approach looking at electrochemical sensors that use PANI, and related polymers; and QCM sensors separately is going to be used.

In the field of electrochemical sensors there are an extremely wide range of possibilities of combinations of conducting polymers and modifications, therefore, to reduce the scope, the search looked for works that used PANI and polypyrrole to sense the concentration of ammonia in the water.

For QCMs, the search was done to works that used QCMs for detecting ammonia in either gases or in water using PANI as a conductive polymer. This is done because no high relevance works have been published using QCMs using PANI/rGO composites for aqueous ammonia detection.

For the detection system, however, an in-depth review was done on other state-of-the-art monitoring systems of simple sensors such as the one seen in QCM's and how they were evaluated.

2.2 PANI-based Aqueous Ammonia Sensors

In the work of (WU et al., 2017), K. Wu et. al. developed a highly sensitive aqueous ammonia sensor using a deposition of PANI on copper and silver wires, with an linear range of $10\mu M - 10mM$ and $100\mu M - 100mM$ respectively. Y.F. Huang et. al. achieved a fast response time sensor $T < 1s$ with linear range of $100\mu M - 100mM$ through the usage of films composed of a copolymer of aniline and 2,5-Dimethoxyaniline and PANI around a silver wire (HUANG et al., 2015). In the work of (KAN et al., 2016), Y. Kan et. al. presents a PANI and poly (o-phenylenediamine) on a silver nanoparticle substrate with a very large linear range for ammonia of $20\mu M - 100mM$ and fast response time T $0.5 - 2s$.

2.3 QCM-based ammonia sensors

In the field of using QCMs in the sensing of gaseous ammonia: In R. Roto et al.'s work, a QCM-based gaseous ammonia sensor was developed by enveloping the QCM crystal with a polyvinyl acetate nanofiber film doped with boric acid. It achieved a detection limit of $650ppb$ (ROTO et al., 2020). In Ying-hu et al's, a polyacrylic acid-doped polyvinyl alcohol nanofiber

film was used on a QCM crystal for gaseous ammonia sensing and a detection limit as low as $100ppb$ was found (HU et al., 2018).

2.4 QCM-based Substance Classification Systems

In X. Su et al.'s work, a QCM-D was used with a coated quartz crystal in multi-resonance mode, obtaining the frequency and dissipation shifts in several harmonics (6MHz, 18MHz, 30MHz and 42MHz), collecting multi-dimensional data used for a classification of several volatile gaseous compounds such as Ethanol, N-heptane, Benzyl alcohol, Acetone, Benzene and others, achieving a 97.5% accuracy (SU et al., 2020). In S. Okur et al.'s work an array of 12 quartz crystals functionalized with 12 different coatings and materials were used for the classification between 6 different mint compounds, after collecting approximately 1800 observations, a KNN and LDA based classifier achieved a prediction accuracy of 90.6% (OKUR et al., 2021). In L. Qiang et al's work, an array of 8 QCM crystals functionalized with 8 different polymer coatings were used in classifying 10 different Chinese liquours and using a multi-dimensional scaling SVM classifier, it was able to achieve a prediction accuracy of 98.3% (LI; GU; JIA, 2017).

3 Theoretical Foundation

3.1 Contamination sensor

3.1.1 Poly-aniline and Reduced Graphene oxide composite sensor

3.1.1.1 Poly-aniline

Poly-aniline(PANI) is an inexpensive and easy to produce conductive polymer that is often used in a multitude of sensors for a variety of different analytes such as Ammonia in both aqueous and gaseous forms (WU et al., 2013) (HADANO et al., 2021) (CROWLEY et al., 2008) (MAITY; MANOHARAN; KUMAR, 2020), chloroform (Mohamad Ahad et al., 2018) and other organic compounds . The main characteristic that drives the wide-spread usage of poly-aniline as an electrochemical sensor is the fact that it has several different oxidation states that present varied physical and electrical properties such as electrical resistance (VIRJI et al., 2004) and shear stress response (FANG; SUNG; CHOI, 2006) conditions that can be distinguished between one another.

The main oxidation states that are pertinent to the usage of PANI as a sensor are the emeraldine base and the emeraldine salt states, shown in Figure 1 (HADANO et al., 2021). This is due to the fact that the presence of a dopant element, such as positively charged compounds or molecules, will reduce the emeraldine-base into the emeraldine-salt form, displaying an increased conductivity and changing its polymeric structure (HADANO et al., 2021). Moreover, if the emeraldine-salt is exposed to a negatively charged ion such as ammonia (NH4), it will oxide back into its emeraldine-base form, lowering its conductivity (HADANO et al., 2021). Since these reactions are reversible in both directions makes this sensor reusable and its measurements repeatable (VIRJI et al., 2004).

The reaction can be seen in Equation 1, one consequence of the changes in PANI's polymeric structure is that its viscoelastic properties will also change. According to (SHAKTAWAT; SAXENA; SHARMA, 2011), PANI in its salt form will have a more rigid nature, while in its base form, it will have a more viscous one (SHAKTAWAT; SAXENA; SHARMA, 2011).

3.1.1.2 Reduced Graphene Oxide

Graphene, a carbon-based structure formed as a two-dimensional honeycomb-shaped lattice built on sp^2 bonds between its atoms, has garnered much interest in recent years due to its unique electrochemical and mechanical properties. Having been used as an electrode in chemical sensors (HADANO et al., 2021), field-effect transistors (FET) (OH et al., 2017), electrodes for super-capacitors (CHEN et al., 2020), and others, Graphene and Graphene-based compounds demonstrate a large array of possible applications and it is mainly due to the fol-

lowing merits (HADANO et al., 2021) (RAY, 2015):

(i) its two-dimensional structure allows most of its carbon atoms to be exposed to the environment to be sensed, maximizing the surface area of the sensor, providing a higher sensitivity to its analytes;

(ii) its inherently low electrical noise due to its high quality pure carbon structure;

Due to those advantages, graphene sheets have been widely studied in composition with other materials such as conducting polymers, metals and metal oxides, and it has been shown that it plays important roles in the improvement of the sensitivity and selectivity of sensors (RAY, 2015).

In its reduced oxidized form, reduced Graphene oxide (rGO) presents many of the aforementioned characteristics in addition to also being able to react with different analytes (RAY, 2015). One common interaction it presents is the reduction of its carboxyl groups due to the presence of negatively charged analytes (RAY, 2015). This reaction is illustrated in Figure 1 and it results in an increase in electrical resistance of the rGO structure (HADANO et al., 2021). The honeycomb structure of rGO is shown in Figure 1 where the carboxyl groups, called the dangling bonds of rGO, are clearly seen in relation to the rest of the structure.

Figure 1 – Notable chemical reactions between rGO and Pani with ammonia

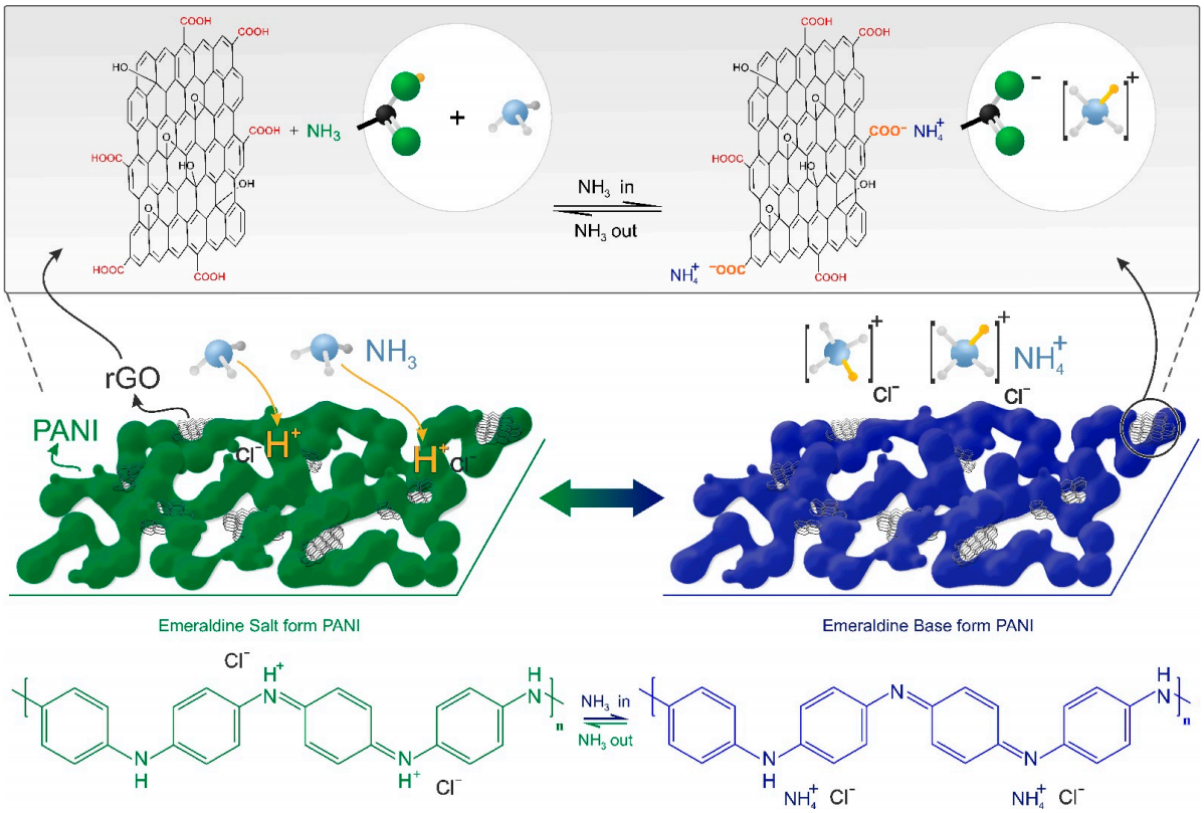

Source: Hadano, Fabio et al (HADANO et al., 2021)

One phenomenon that has been studied in rGO and its non-reduced counterpart (Graphene Oxide) is its semi-conductive behavior, showing much of the same characteristics as a p-type semiconductor, meaning that the decrease in electrical conductivity of the rGO chain, through its interaction with negatively charged particles, can be, in part, explained through the removal of majority charge carriers (protons) (MAJUMDAR; BASKEY; SAHA, 2011). This effect is a possible explanation as to why the addition of rGO in composite materials leads to an improvement of their selectivity and sensitivity to certain analytes through the enlargement of depletion layers in semi-conductive hetero-junctions formed by rGO and the other material in the composition 3.1.1.3 (MAJUMDAR; BASKEY; SAHA, 2011).

3.1.1.3 Poly-aniline/Reduced Graphene Oxide Composite

The composition of PANI and rGO has been studied under a myriad of different settings, having been applied in fields from the creation of films for flexible super-capacitors (CHEN et al., 2020), to sensors for humidity (LEE; WANG, 2019) and ammonia (HADANO et al., 2021) in gases, the composite presents a variety of interesting features such as an improved sensitivity in relation to PANI (HADANO et al., 2021)(HUANG et al., 2012) (WANG et al., 2019), good energy storage (WAN; JIAO; LI, 2017), good sensing performance at room temperature and improved sensing abilities like response time, recovery time, and others (LEE; WANG, 2019).

These features can be said to hail from different synergistic interactions between rGO and PANI, the most important of which are (HADANO et al., 2021) (MAJUMDAR; BASKEY; SAHA, 2011): (i) the presence of similar interactions with analytes; (ii) the formation of electronic hetero-junctions at interfaces and (iii) the electric characteristics of rGO.

Starting from the similar interactions, as it has been described in Sections 3.1.1.1 and 3.1.1.2, both rGO and PANI react spontaneously with ammonia in the water due to the similar dangling-bond structures of the Carboxyl groups from the rGO structure and the emeraldine-salt. By having similar interactions, the composition of rGO into PANI will not have any detrimental effects in its sensing capacity (HADANO et al., 2021).

In addition, as it was shown in (MAJUMDAR; BASKEY; SAHA, 2011), the interface between rGO and PANI presents Schottky hetero-junctions that will create conductive and depletion regions at the interfaces and the addition of analytes, such as $NH3$, to those hetero-junctions will increase the size of the depletion regions, increasing drastically the electrical resistance of the composite (MAJUMDAR; BASKEY; SAHA, 2011). Moreover, as it was discussed in Section 3.1.1.2, rGO has an exceptionally high conductivity, improving its ability to be added to other sensors without a detriment to their sensitivities (HADANO et al., 2021).

3.1.2 Quartz Crystal Microbalance

Quartz Crystal Microbalance (QCM) devices are sensors that have the ability to measure characteristics such as weight at a scale of nano-grams (LIU; ZHANG, 2013) and are

commonly employed to measure physical properties such as density, viscosity, elasto-viscosity of polymers in different environments (LIU; ZHANG, 2013). By having the hability of measuring such properties, by adding an adsorbed layer of molecules that interact with specific foreign objects like other molecules or organisms such as protozoa, cells and other microorganisms, changes in weight can be infered as interactions between the adsorbed layer material and the environment, which can be used to detect the presence of a certain microorganism in the environment (VAUGHAN; O'SULLIVAN; GUILBAULT, 2001). This is extremely useful for the detection of common food pathogens in solutions, common water contaminants, the study of the interactions between immuno-bodies and certain microorganisms (YILMAZ et al., 2015) (VAUGHAN; O'SULLIVAN; GUILBAULT, 2001) (CHEN et al., 2016) and the study of nanoparticle depositions (CHEN et al., 2016).

3.1.2.1 Working Principle

The main working principle of Quartz Crystal Microbalance systems is based on the concept of Piezoelectricity, the property of a material being able to physically vibrate through the injection of electrical current, commonly also used to generate electrical signals through the physical deformations of the material (LIU; ZHANG, 2013) (CHEN et al., 2016). These Piezoelectric materials, when under the influence of alternating currents, have a frequency response with a resonant frequency that's ultrasensitive to elements such as changes of mass adsorbed to the crystal, temperature changes, and changes in the viscoelastic properties of the film coating the crystal (if pressent) (LIU; ZHANG, 2013) (CHEN et al., 2016).

The changes in the resonant frequency are dictated by different equations depending on the setup of the crystal. If the crystal is placed under a gaseous environment, it can be simply described by the Sauerbrey equation, shown in Equation 3.1 (CHEN et al., 2016),

$$\Delta f = -\frac{2f_0^2}{A\sqrt{\rho_q \mu_q}}\Delta m \tag{3.1}$$

Where f_0 is the resonant frequency of the crystal, A is the surface area of the crystal and ρ_q and mu_q are the crystals density and shear modulus respectively. With the variables f_0, A, ρ_q and mu_q being approximately constant, they are usually condensed into only one constant value (CHEN et al., 2016) (LIU; ZHANG, 2013).

$$\Delta f = -C_f \Delta m \tag{3.2}$$

Meaning that a change in resonant frequency of the crystal is directly and linearly related to a change in mass under the specific regime specified earlier. However, these equations are very limited though, showing severe disparities when placing or flowing a liquid on the crystal. This has been resolved by the Kanasawa Gordon equation shown in Equation 3.3 (LIU; ZHANG, 2013).

$$\Delta f = -f_u^{3/2} \sqrt{\frac{\rho_L \eta_L}{\pi \rho_q \mu_q}} \tag{3.3}$$

This Equation is used when the clean crystal is under liquid conditions, with ρ_L being the density of the liquid and η_L being the liquids viscosity. This means that we can differentiate different liquids through the differentiation of the different frequency responses associated with the characteristic $\rho_L \eta_L$ of each liquid.

Another equation that can be used is the Butterworth Van Dyke equation, presented in Equation 3.4 (LIU; ZHANG, 2013) that's based on the Butterworth Van Dyke model of a quartz crystal, it also only is valid when the crystal is clear.

$$\Delta R = \frac{n \omega_s L_u}{\pi} \sqrt{\frac{2 \omega_s \rho_L \eta_L}{\rho_q \mu_q}} \tag{3.4}$$

Where n is the oscillating mode of the crystal, $omega_s$ is the unloaded resonance frequency and L_u is the inductance of the resonator. This will be used to also characterize different liquids through the product of $\rho_L \eta_L$.

The measurement of the series motional resistance is done indirectly through the relation given by the equivalent resonant oscillating circuit, shown in Figure 2. It assumes that the oscillator has a total phase shift of 360° and a unitary gain in order to have the relation shown in Equation 3.5 (STANFORD, 2004).

Theoretically asserting that the electrical resistance of the material on adsorbed to the crystal has no effect on the resistance measured by the device, except in cases of correlation between electrical resistance and viscoelastic properties of the material.

Figure 2 – Equivalent circuit of the oscillator at series resonance.

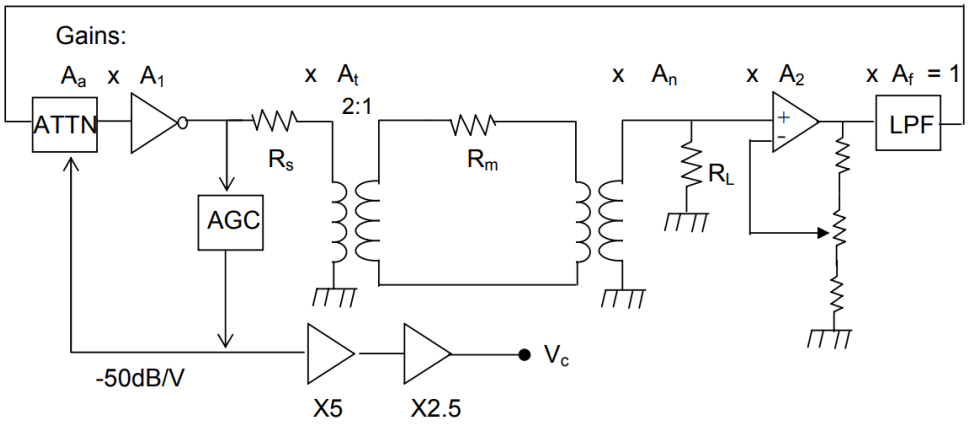

Source: Stanford Research (STANFORD, 2004)

$$R_m = 10000 \times 10^{-V_c/5} - 75 \tag{3.5}$$

Although the system has a strong mathematical foundation, the crystals themselves will show a change in their physical properties based on pressure, temperature, and pressure and temperature hysteresis effects that are not yet well understood, some probable causes of those effects can be a redistribution of contaminants in the crystal enclosure, hysteresis or thermal gradients (STANFORD, 2004).

Experimentally, these hysteresis effects will lead the sensor to have a considerable amount of drift in its measurements, leading to inaccuracies in its readings depending on temperature drifts, sudden temperature fluctuations. The expected drift in the measurements are given by the Equations 3.6 and 3.7 where ΔT is the fluctuation in temperature, while Δf^* and ΔR^* are the expected Frequency and Resistance fluctuations based on temperature respectively.

$$\Delta f^* = 8 * \Delta T \tag{3.6}$$

$$\Delta R^* = -4 * \Delta T \tag{3.7}$$

Besides those disparities, when the crystal has a film placed on its surface, the changes in frequency and motional resistance are no longer associated directly with the viscosity of the fluid it is inserted in, instead, it is strongly associated with the viscoelastic properties of the film itself (ARUGULA; SIMONIAN, 2016), being sensitive to changes in the polymer's thickness, roughness, viscoelastic changes, material adsorbtion, and other external factors (ARUGULA; SIMONIAN, 2016). Due to these effects, most QCM-based sensors are better suited for detection tasks instead of measuring concentrations precisely.

One way to see the association between the viscoelastic properties of a material is associated with the readouts from the QCM is through the Butterworth-van-dyke model of shear stress in the crystal, shown in relation to the motional resistance in Equation 3.8 (JOHANNSMANN, 2007).

$$R1 = \frac{d_q^2}{8A_q e_{26}^2} Z_q n \pi tan(\delta) \tag{3.8}$$

Where all parameters with the subscript q are the constant parameters of the crystal, d_q being the thickness, Z_q the impedance and A_q the area of the crystal, besides those, e_{26} is the constant piezoelectric stress coefficient and n is the overtone order, which for the purposes of the $5MHz$ crystals used for this project, it is approximately 1, lastly, $tan(\delta)$ is the related to the ratio of the loss modulus (G'') by the storage modulus G' of the film, according to Equation 3.9 (JOHANNSMANN, 2007).

$$\tan\delta = \frac{G''}{G'} \tag{3.9}$$

Figure 3 – Samples from the dataset built from the experiments performed

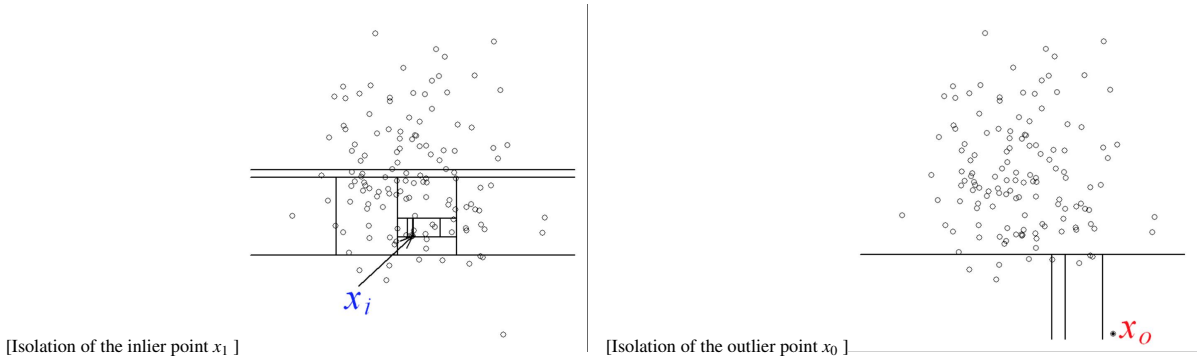

[Isolation of the inlier point x_1] [Isolation of the outlier point x_0]

Source: Liu Et. Al (LIU; TING; ZHOU, 2008)

Based on that, it can be said that the resistance of the material is directly proportional to its loss modulus and inversely proportional to its storage modulus based on that equation. Therefore, if the resistance is higher, it means that the film presents a more viscous nature, otherwise, it would be evidence for the film presenting a rigid structure (JOHANNSMANN, 2007).

However, coating the crystal with an external sensitive film adds in the complexity of the sensor system as a whole, by adding the sensitivities of the film to the realm of deviations and drifts the sensor might have, one common of which one is sensor degradation, where the film itself will degrade and have its viscoelastic and sensitive properties changed, causing a permanent drift in the measurements of the sensor (ARUGULA; SIMONIAN, 2016). These types of drifts are film-specific, therefore largely cannot be avoided without changing the setup of the experiment or the film itself.

3.2 Contamination Detection Algorithms

3.2.1 Isolation Forest

In order to describe Isolation Forests as anomaly detection algorithms, it is first necessary to describe Isolation Trees, their main component parts. Isolation trees are structures that, at each node, will divide the feature space into two sections at a point q where one section is comprised of the points p where $p(q) < q$ and the other one where $p(q) \geq q$ (LIU; TING; ZHOU, 2008).

If each point has an approximately unique set of tree nodes that describe its position within the feature space, then it means that Isolation Trees are able to give approximate positional representations of those points based on how the path taken through its nodes. One consequence of this is that the more sparsely the points are distributed, the less nodes it will needed to spacially represent it within a tree, thus the shorter the path length of its representation, the more distant it is from other points in the feature space, and the more likely it is an anomaly (LIU; TING; ZHOU, 2008). A visual representation of this effect in shown in Figures 3 and 3

Figure 4 – Convergence of the average path length through the combination of isolation trees.

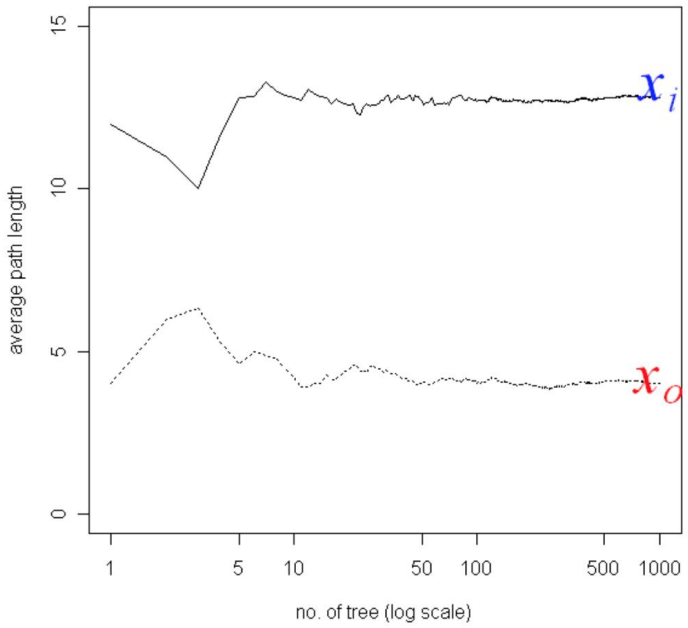

Source: Liu, et. al. (LIU; TING; ZHOU, 2008)

The number of nodes needed to traverse the tree in order to get to a point p is denominated its "path length"$P(p)$ (LIU; TING; ZHOU, 2008).

In order to train the trees, a preprocessing step is needed on the points present in the features space. They first need to be subsampled, having the number of points in the feature space limited to a set amount ϕ. This is done to reduce the model complexity and to avoid the swamping effect, caused by the presence of anomaly clusters that might have long path lengths that might be mistaken as normal data points (LIU; TING; ZHOU, 2008).

Then the trees are trained by, starting at the root node, selecting a random feature of the feature space and choosing a point q that sits between the minimum and maximum of the points within that feature and diving the space between two nodes points smaller than q and greater than q. This is done recursively for each node created until the node cannot divide anymore for only having one data point, or for having reached the maximum allowed height for the tree (LIU; TING; ZHOU, 2008).

Combining these trees into an ensemble of forests, an Isolation Forest is created. By averaging the path lenghts of a specific point for all trees in the forest, it is seen that its value will converge to one specific number, as seen in Figure 4, larger for normal points and smaller for anomalous points, creating a metric that can be normalized into an anomaly score. Providing a solid foundation of an unsupervised anomaly detection algorithm that could also be utilized as a contamination detection system (LIU; TING; ZHOU, 2008).

The algorithm does have its shortcomings, however. Its training step requires a subsample of the entire dataset, without regard to the possibility of local anomalies within the dataset,

being less appropriate for its usage in datasets with highly contextual anomalies (GAO et al., 2019). However, because of its simplicity, linear time complexity and low memory requirements, the isolation forest algorithm remains a widely used algorithm for anomaly detection in several use cases (GAO et al., 2019).

3.2.2 One Class SVM

Regular Support Vector Machines (SVMs) are widely used in regression and classification problems, however, they lack the ability to adapt to highly unbalanced datasets such as is the case for anomaly detection datasets cases where the number of anomalous cases, by their very nature, is extremely small in comparison to the number of regular data points. One class SVM or OCSVM works on the fundamentals of regular SVMs for those specific cases.

The OCSVM algorithms work on the basis of fitting a hyperplane or hypersphere in the data points' feature space in order to encompass all of the data points. For any new data points p, their anomaly score will be based on where it lies in relation to the fitted hyperplane.

Figure 5 – Comparison of different ν values for the SVM classifier

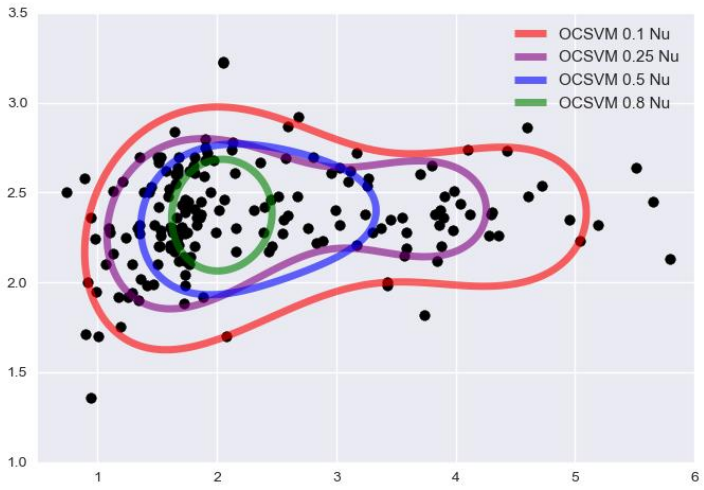

Source: Scikit-learn (PEDREGOSA et al., 2011)

The hyperplane that dictates the decision boundary of OCSVM algorithsm is similar to the ones in SVM classifiers, in which they both require a kernel function in order to separate non-linearly separable partitions of the dataset. A few common ones that are commonly used are the linear, sigmoidal, polynomial and rbf kernels, their distinct effects on the output of the SVM classifier is shown in Figures 6,6,6, and 6 respectively.

When the OCSVM algorithm is used for outlier detection, it utilizes the hyperparameter of "contamination"(ν), that dictates the percentage of the dataset that is expected to be an anomaly, a larger value will lead it to separate more of the input dataset as an anomaly, as it is seen in Figure 5.

Figure 6 – Samples from the dataset built from the experiments performed

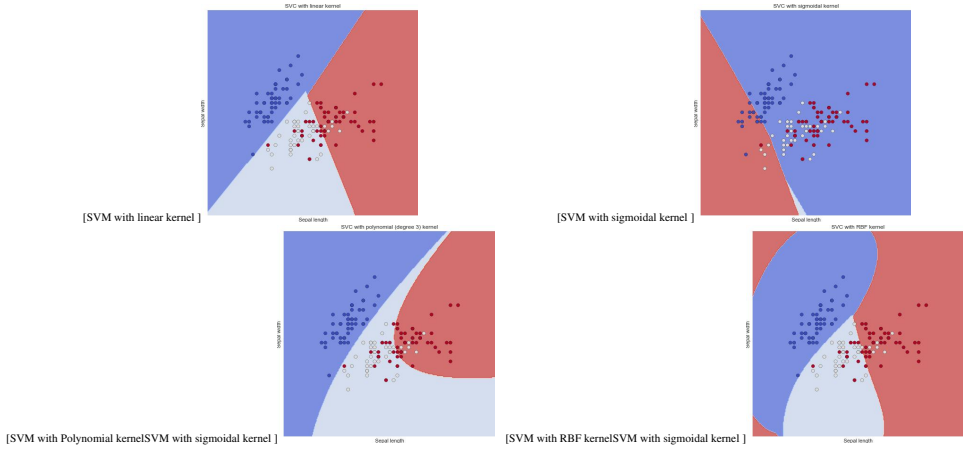

Source: Scikit-Learn (PEDREGOSA et al., 2011)

3.2.3 Holt Winters Forecast Error

Different from the other anomaly detection techniques, Exponential Smoothing (ES) forecast anomaly detection techniques are based on the concept of "forecast error", in which, by making a prediction of how a time series will behave in the future and comparing it to the actual values, it is possible to detect which data points are behaving in an unexpected way to what it has been seen until that point.

The way in which the ES algorithms generally work is through the usage of the simple weighted average of previous values, such as is defined in Equation 3.10, where $y'(t)$ is the smoothed/expected value of $y(t)$, and α is the exponential decay coefficient of the system. The output of this system and its forecasts are shown in Figure 7.

$$y'(t) = \alpha y(t-1) + (1-\alpha)y'(t-1) \tag{3.10}$$

This concept is then expanded upon by the Holt Winters model, that uses the principle of Exponential Smoothing to make predictions on the average level of the data, its trend component, as well as its seasonal component in order to predict its output. Its base equations in its additive form are shown in Equations 3.11, 3.12, 3.13 and 3.14.

$$l_t = \alpha(y_t - s_{t-m}) + (1-\alpha)(l_{t-1} + b_{t-1}) \tag{3.11}$$

$$b_t = \beta(l_t - l_{t-1}) + (1-\beta)b_{t-1} \tag{3.12}$$

$$s_t = \gamma(y_t - l_{t-1} - b_{t-1}) + (1-\gamma)s_{t-m} \tag{3.13}$$

Figure 7 – Effects of different levels of α in the predictions by a simple exponential smoothing forecaster

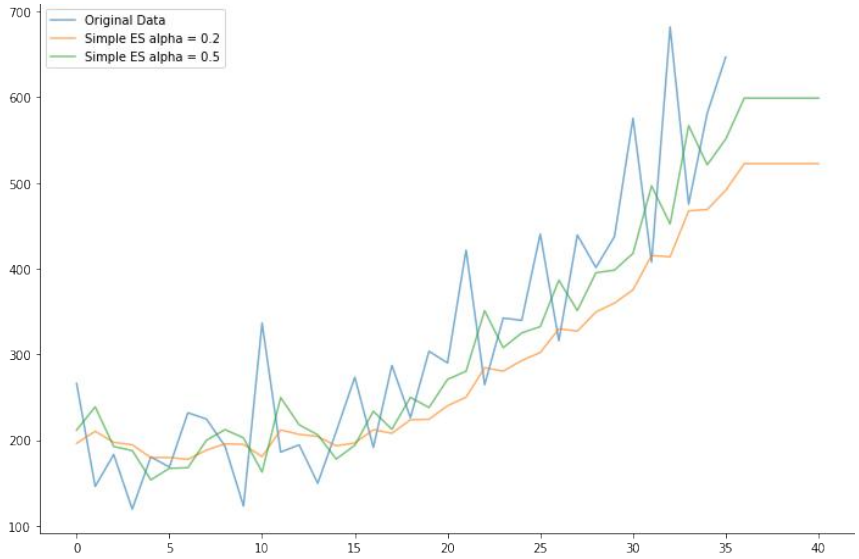

Source: Self authorship

$$y'_t = l_t + hb_t + s_{t-m+h} \tag{3.14}$$

Equation 3.11 describes the exponentially smoothed level l_t of the data, where s is the seasonality, t is the current time-step, m is the period of seasonality, b is the trend component and α is the level decay coefficient.

Equation 3.12 defines the trend component by the difference of the two previous values of the level component (similar to a derivative), β is the trend decay coefficient.

Equation 3.13 defines the seasonality component of the holt winters model and it separates the actual value from the predicted trend and level component in order to create an exponentially smoothed estimation of the seasonality of the data.

Lastly, Equation 3.14 combines all components into one equation, where h is the forecast horizon. With this, it is possible to create more accurate predictions of the data by tuning its different values of α, β, γ and m. For non seasonal holt-winters models, tuning the γ and m are irrelevant, however. An example of the output given by a Holt Winters model can be seen in Figure 8.

By comparing the error between the forecasted values with the actual values seen, it is possible to obtain an error metric of how unexpected the actual value is based on the data seen up until now, being able to be used as an anomaly detection algorithm.

Figure 8 – Forecasting of the same data in Figure 7 with the holt winters model

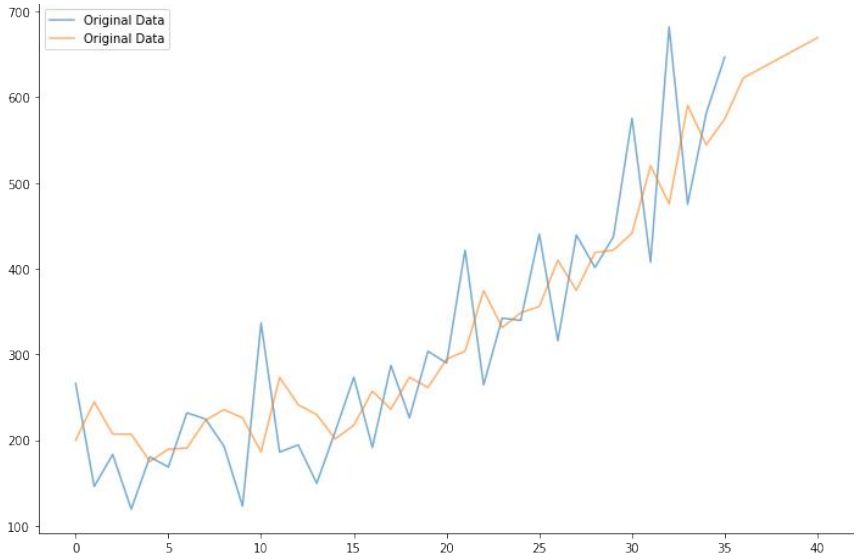

Source: Self authorship

4 Methodology

4.1 Specifications and Requirements

The functionalities described in this section is related to the objectives listed in Section 1.2, so that each one of them are properly achieved.

1. **To develop an experimental setup for QCM measurements of different substances**
   - FR01: The experimental setup must be reproducible within separate days;
   - FR02: The experimental setup must be suitable for monitoring of a control substance;
2. **To define control measures in order to validate the experiment**
   - FR03: The system should have a defined contamination threshold over which all contaminations must be detected;
3. **To identify the best detection method of contaminations**
   - FR04: This report must have a well-defined justification as to why the detection method was chosen and through which metrics it was evaluated as being sufficient;
     - In order to reduce the scope of this statement, as to not compare every detection method in existence, a particular set of detection methods was used for comparison and the results are shown in Section 5.2.1.1
4. **To develop a detection model for the contaminants**
   - FR05: The detection model must have a surrounding graphical user interface (GUI) in order to collect the measurements;
   - FR06: The detection system around the detection model must notify its users that a contamination was detected;
5. **To test and evaluate the contamination detection model**
   - FR07: The detection model must be able to detect all contaminants above a certain contamination threshold.

To further specify some of the functional requirements, they were broken down into subrequirements as follows:

- FR05.1: The GUI must have a button and selector combo for the incoming data port;

- FR05.2: The GUI must have a button and selector combo for the output data path;
- FR05.3: The GUI must have a button and selector combo for the notification route;
- FR06.1: The user can toggle on and off the notifications from the system as needed;
- FR06.2: The user can provide an email to be registered for it to be used for any notifications;
- FR06.3: The system must notify the user if any contaminations have been detected.

4.2 Project

The project was divided into two main components, the measurements and validation of the QCM sensor system and the development of the contamination detection system. Since these two are separate components, they were assigned to the measurement phase and the development phase of the project.

4.2.1 Measurement Phase

During the measurement phase, the sensor system were validated through repeated experiments with increasing concentrations of contaminants, starting from a concentration that is well below the limit imposed by external authorities, up to the concentration at which it is deemed that the sensor has gone well past what would be feasible for it to be found in normal environments.

Using this test methodology, the response of the sensor to an increase in contaminants can be assessed at all normally/naturally attainable concentrations and, by analyzing the overall response of the sensor, a limit of detection can be obtained and the response characteristics of the sensor can be used in order to develop the contamination detection software.

Before this can be achieved, however, a standardized test setup/test workbench needs to be devised so that the system can be repeatable through different days and even different seasons.

4.2.2 Development Phase

During the development phase, the detection model and the detection system around the model was developed using the data that was collected during the measurement phase as guides in order for them to be in accordance to all of the requirements given by Objective 4. described in Section 4.1.

After this development phase, an evaluation phase was performed, evaluating whether or not the requirements set by Objective 5. described in Section 4.1 were met with the system that was developed.

Through preliminary results of the QCM in different test conditions, it can be seen that the output of the sensor suffers from significant drift depending on test conditions such as temperature and immersion depth, therefore, the detection system must take into account two extra conditions for its operation:

- FR07.1: The Detection system must take into account the measurement drift between measurements;
- FR07.2: The Detection system must be resistant to measurement drifts within one measurement

Thus the detection system must take into account if there are any temperature changes between different measurements and changes in the test conditions while the system is running, such as gradients in the ambient temperature, temperature differences between the crystal and water, etc.

4.3 Architecture

The architecture of the detection system follows a standard Model-View-Controller (MVC) Architecture, this is further described in Section 5.2.3, however, the main part of its core functionalities can be visualized in the Diagram shown in Figure 9.

Figure 9 – MVC-based architecture of the detection system

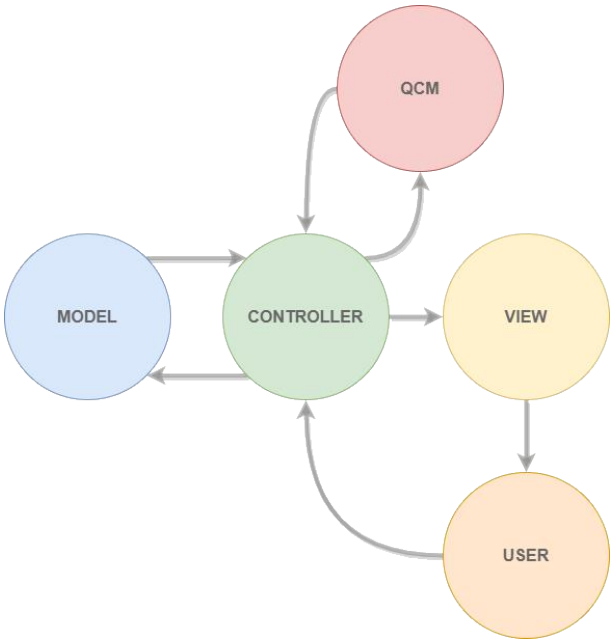

Source: Self authorship

In this architecture, there are 3 main components: (i) the View (ii) the Controller and (iii) the Model. Starting from the View, it is the Graphical component of the system, the UI,

buttons and other elements with which the user is able to interact directly with the system. Usually this component is fused together with the Controller, who is the component that deals with the internal logic of the system, like the internal state of the user interface, reading user inputs, calling functions from the View component in order to update the user's interface due to an outside action and performing external actions such as API calls.

Lastly, there's the Model, in which the internal logic around data components is handled, this is where the detection model is stored, through which the controller knows whether or not there has been a contamination in the previous sample collected. Furthermore, behind the model there is an evaluation component, that uses the detection model in order to test it with every sample, and with it, the evaluation component provides the recall metric for the detectors tested.

5 Development and Results

5.1 Measurement Phase

5.1.1 Synthesis of the Sensor

In order to start the measurements, we first needed to synthesize the film polymer composite, to do that, first, using a *Marte Shimadzu AY220* scale, shown in Figure 10, a 4:1 ratio of PANI to rGO was measured into a *polytetrafluoroethylene* covered vial. This mixture was then dissolved into $100\mu L$ of N-Methyl-2-pirrolidone (NMP) in order to make an suspension of small and large pieces of rGO in a PANI solution.

Figure 10 – Scale used in this project

Source: Self authorship

One of RGO's defining traits, as explained in Section 3.1.1.2, is that it increases the surface area of the sensor, increasing its sensitivity, while also increasing its selectivity, however, the larger pieces present in the suspension will decrease its overall surface area, leading to worse results as a sensor. In order to circumvent this, the suspension was put into an ultra-sonic bath for 20 minutes, making the larger pieces sink more readily towards the bottom of the vial, effectively separating the pieces from one another.

After this procedure, using a TopScien $10 - 100\mu L$ micropipette, $100\mu L$ from the top part of the vial, where the smaller particles were suspended, was separated out and deposited on the QCM crystal through spin coating. The resulting film has a blue and purple tonality, with a few darker specks, which indicates that the PANI and rGO mixture has been deposited properly.

The resulting sensor can be seen in Figure 11a, and a diagram with the respective components of the sensor are shown in Figure 11b.

Figure 11 – The coated Quartz Crystal Microbalance Sensor

(a) Sensor coated with PANI and rGO

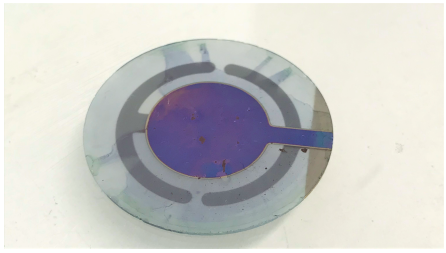

Source: Self authorship

(b) A rendered 3D model of the sensor

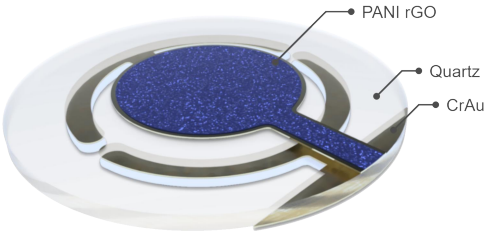

Source: Self authorship

In order to see the morphology of this sensor, it was put through a *Taylor Hobson CCI MP* profilometer and the resulting image was processed using the MountainLabs 9 software, the results can be seen in Figure 12, where it can be seen that the overall profile of the PANI/rGO film contains a significantly rough nature to it, possibly indicating an increase in surface area in comparison to pure PANI films (HADANO et al., 2021).

Figure 12 – Morphology analysis of the sensor synthesized

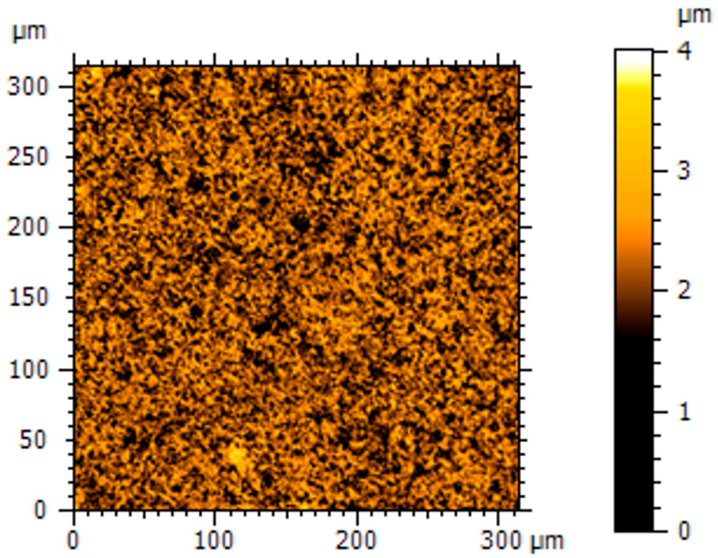

Source: Self authorship

5.1.2 Defining Control Measures

In order for this project to have a meaningful point of comparison with regulations and with current literature standards of ammonia detection and sensing, one of the objectives of this project is to define a control measure of what concentration of ammonia would be considered to be the minimum that the system needs to be able to detect 100% of the time.

To do this, firstly, regulations on ammonia regarding health and safety were surveyed, and, according to the U.S. Environmental Protection Agency (EPA), chronic exposure of ammonia, one that exceeds 30 days, is prejudicial to most aquatic life when in concentrations of over $1.9mg/L$ (HUFF et al., 2013). Acute exposures, ones of approximately 1 hour, only show prejudicial effects when in concentrations of over $17mg/L$.

For humans, the concentrations in which these effects can be seen is in the case of drinking water, where a concentration of over $23mg/L$ has shown effects of irritability and lethargy in infants (KNOBELOCH et al., 2000). However this can be seen as an extreme case of ammonia poisoning, in most cases, ammonia is not harmful to humans, but its presence in clean water usually is a direct sign of external contamination (HUFF et al., 2013).

In other systems, ammonia can be an extremely toxic substance, according to the UN Food and Agriculture Organization, some species of Cyprinid fish are sensitive to ammonia concentrations as low as $1.0mg/L$ and Salmonids to concentrations of $0.5mg/L$ (SVOBODOVÁ, 1993).

Besides the regulations already in place, the state of the art must also be taken into account in order to define what the threshold must be. As was seen in Section 2, some PANI-based electrochemical aqueous ammonia sensors works since 2015 have had their data summarized as seen in Table 1 where the Limit of Detection (LOD) and Range of Operation (Range) were converted from μM to mg/L for consistency in the data.

Table 1 – Table of similar aqueous ammonia sensors since 2015

Active Sensor	Range (mu M)	Range (mg/L)	LOD (mu M)	LOD (mg/L)	Ref.
PANI/Ag.	10 - 10000	0.18 - 180.39	-	-	(HUANG et al., 2015)
PANI/Ag. wire	100 - 100000	1.8 - 1803.9	-	-	(WU et al., 2017)
PANI/Ag. nano wire	20 - 100000	0.36 - 1803.9	12	0.216	(KAN et al., 2016)

It is important to note that the LOD is only an estimation of how low the concentration of the analyte can get before it merges with its background noise (ANDERSON, 1989), therefore it does not directly provide the control measure needed.

One way for the control measure to be defined is for it to be within the range of all of these past works, having assumed that the sensor synthesized has similar characteristics. Being based with PANI and an external conductive material, it would be safe to say that the PANI/rGO sensor's operational range will include $1.9mg/L$, which is the upper limit for the acceptable concentration of ammonia in water according to the EPA. Therefore, it can be used as the control measure of this project, meaning it will be used as a threshold, over which all contaminations must be detected.

5.1.3 Test Setup

In order to test the sensor, a test setup needs to be developed and tested, from what is seen in the manual from the QCM200, two different setups for testing the sensor are appropriate:

(i) static and (ii) dynamic setups.

(i) Static setups require simply a volume of liquid in which the sensor can be immersed in and a contaminant can come into contact with the liquid and spread out, coming in contact with the sensor(STANFORD, 2004);

(ii) Dynamic setups on the other hand is reliant on mechanical systems to push liquids through a flow cell that guides liquids through the surface of the crystal, in order to insert controlled contaminants, a multi-port flow valve is needed to modulate the flow from the various pumps to continuously push liquid through the flow cell. A diagram of this system is shown in Figure 13 (STANFORD, 2004).

Figure 13 – Diagram of a dynamic test setup

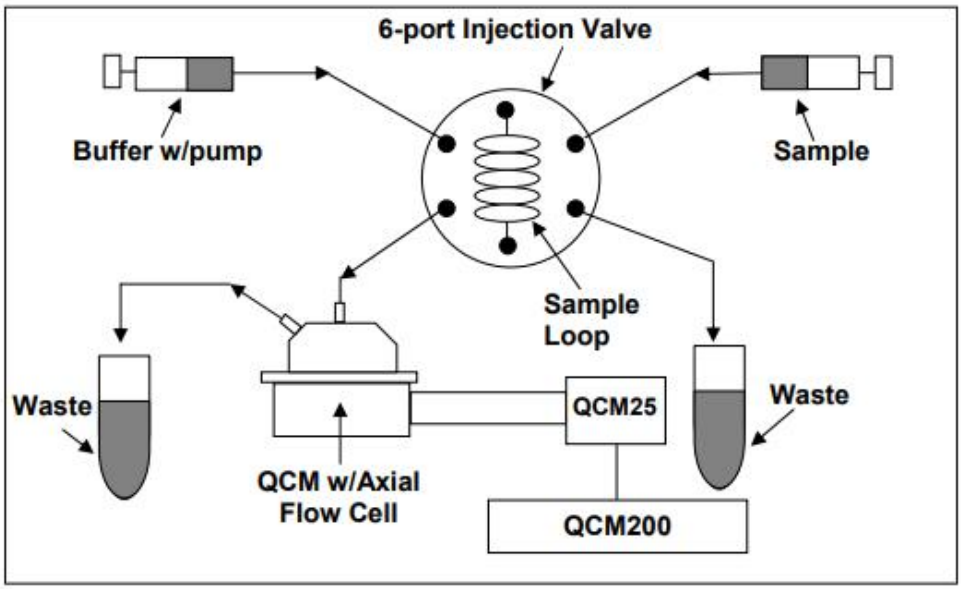

Source: Stanford Research (STANFORD, 2004)

Dynamic setups, however, have a large amount of issues associated with their implementation that were raised within the development of this project, a few of them are listed below:

i There is a large amount of mechanical parts

- The large large amount of moving parts attached to the QCM sensor made the sensor readings very unstable when there were unexpected stoppages in the system and due to the pressure hysteresis effect explained in Section 3.1.2, this leads extremely unstable results (STANFORD, 2004).

ii The flow needs to have constant flow, and no bubbles

- The flow recommended for this sensor is of around $0.15mL/h$ (STANFORD, 2004), which requires syringe pumps and surgical tubing for connecting the pumps, which

usually lead to bubbles forming within the tubes or air pockets within the flow cell itself, which requires a reset of the entire experiment.

iii Temperature gradients are amplified

- Due to the movement of the liquid, any temperature changes in the environment leads to a faster, more abrupt response of the sensor. Furthermore, differences in temperature between the liquid and the sensor will also cause large drifts in readouts from the sensor.

Due to these added complexities, the Static setup was chosen for this project, it consists in a beaker filled with the control liquid, distilled water, in the case of this experiment, and the head of the QCM holder, shown in Figure 14, is immersed in it for the duration of the experiment. Any contaminants to be inserted in this mixture are inserted after a set period of time into the water and it diffuses into the rest of the solution.

Figure 14 – The Crystal Holder used for the project

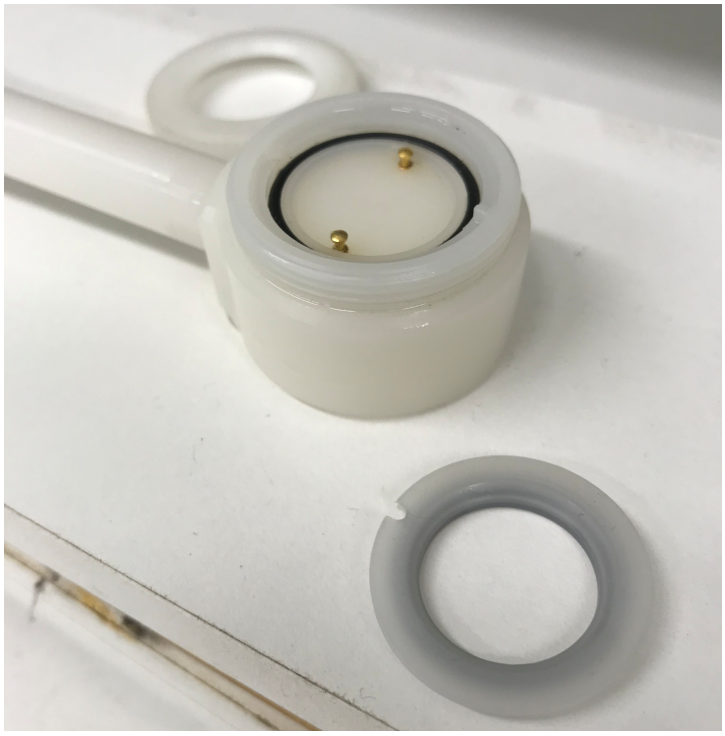

Source: Self authorship

To build the setup, the holder was attached to a raised rubberized clamp and was hung head-first into the beaker for testing, the height was adjusted in order for it to be immersed in a way that it covers the entire crystal holder head. The entire setup with a clean CrAu crystal can be seen in Figure 15.

As for the insertion of the contamination, ammonia needs to be introduced to the system, in order to do this, concentrated ammonium hydroxide (NH_4OH^-) would be inserted into the

Figure 15 – Final setup for the static experiments

Source: Self authorship

water of the beaker, the quantity inserted would be able to modulate the concentration of the mixture according to the following instructions:

5.1.4 Building a dataset

To perform the tests needed for the development phase of this project, a set of controlled experiments must be performed, the main requirements needed for the dataset are the following:

- At least one experiment for each relevant concentration beginning on a value smaller than the control measure and ending in a value high enough to ensure that sensor saturation is not an issue;
- At least one experiment of a blank insertion, in order to ensure that the act of inserting something into the water is not affecting the sensor or the detection model in any meaningful way.

With this, the requirement for FR07 from Section 4.1 can be tested and the low threshold ammonium concentration detections can be verified against the blank insertions in order to ensure that the contamination detection mechanism does not have a significant amount of measurement bias associated with it, in other words, ensure that the detection model is not simply detecting the act of inserting something into the water.

5.2 Development Phase

5.2.1 Contamination Detection Model

The contamination detection model was developed with the requirements set in Section 4.1 in mind. It consists of a combination of several models developed to detect changes in the readings from the QCM200.

5.2.1.1 Algorithm implementation

The algorithms chosen needed to be able to detect the sudden change in the readings of resistance and frequency, as well as to be able to adapt to any measurement drifts that could occur within a single measurement or between different measurements. Taking inspiration from the field of real-time unsupervised anomaly detection algorithms, the ones selected were the One class Support Vector Machine (OCSVM), Isolation Forest, Exponential Forecast and Mean deviation anomaly detection algorithms.

The **OCSVM**, and **Isolation Forest** algorithms were chosen for being well known algorithms that are widely used in the field of real time anomaly detection, however, they suffer in terms of model complexity and processing time in the context of the problem at hand (AHMAD et al., 2017) (LAVIN; AHMAD, 2015).

They were both implemented using the Scikit learn package from python. In order to run the preliminary test performed, the default parameters of both the Isolation Forest, as well as the OCSVM algorithms were utilized, which implies the following parameters:

- OCSVM
  - **Kernel**: Radial Basis Function
  - **Gamma**: Scale
  - **Tolerance**: 0.001
  - ν: 0.5
- Isolation Forest
  - **Isolation Trees**: 100
  - **Sampling size**: Using all samples
  - **Contamination**: Automatic
  - **Number of features**: 2 (Frequency and Resistance)

Prior to its inclusion in the model the data was first preprocessed by taking the difference/derivative between the current data points with the average of 180 seconds in the past.

This normalizes the data to some extent, and taking using the difference in the model aids it in reducing the effects of smoother measurement drifts while also amplifying short term deviations of the data, this effect can be seen in Figure 16.

Figure 16 – Example of the advantages of preprocessing with a 15 minute deviation

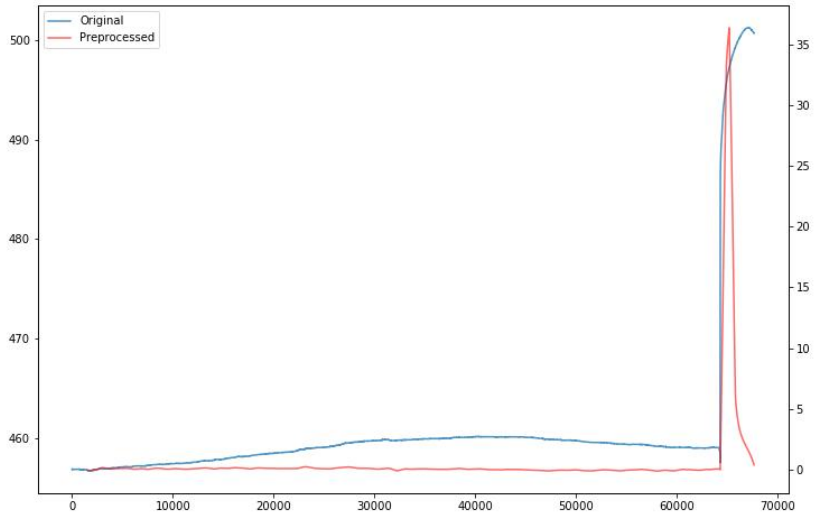

Source: Self authorship

When the system reaches at least 5 minutes worth of data, it fits the models to the collected resistance and frequency measurements, creating the fitted models for the OCSVM and Isolation Forest Algorithm.

After that, after every minute of data collected, these models are used to predict whether or not the newly collected data is anomalous or not. If so, it returns a list of the detections made.

The Exponential Forecast, described in Section 3, is used every minute to predict how the data will behave in the next time step. To do this, the statsmodels module from python was used in order to implement an additive non-seasonal HoltWinter model.

At every detection step, the model is fit to the newly seen data and is used to forecast the next minute of data. When this minute passes, the new data collected is compared to the previous forecast and if the deviation between theses two values exceeds 1% (defined as so due to the results seen in Section 6), that data point is classified as an anomaly.

Lastly, the **mean deviation** algorithm is an extremely simple algorithm that was made using the results obtained from the early tests performed for this project, and it strictly only uses the QCM's resistance measurements for its contamination detection.

It consists of the calculation of a large window moving average of the data. This averaged data is then used by calculating the deviation of the current resistance value with the

resistance measured 15 minutes prior, if this operation results in a deviation larger than 1.5%, an anomaly is detected.

The numbers relative to the 1.5% threshold and 15 minutes are based on the response and rise-time values seen in Section 6.

5.2.1.2 Model Implementation

The proper model implementation is composed of an ensemble of at least two of the algorithms discussed previously, when only one model detects an anomaly/contamination, it is considered a 'probable' contamination, when more than one detects a contamination within a certain time limit (set to 5 minutes in this project), a 'severe' contamination is detected. Which algorithms are going to be chosen for this ensemble is discussed in 6.

The main motivating factor for this type of model is that it is necessary to avoid false negatives as much as possible, while also avoiding false positives. And when employing multiple models with different operating principles at a time, false negatives are less likely, and false positives can be classified differently at the stakeholder's discretion.

To implement this model, separate classes were developed to implement each algorithm explained in Section 5.2.1.1, each of them is connected to the **DetectionVoter** class that is responsible for joining together all of the detections made from each other detector and merging them into one single list of detections that can be used by the **RunController**.

The **DetectionVoter** class is also responsible for fusing together detections made in quick succession and merging several "Probable"contamination detections into one "Severe"detection.

5.2.2 Email Notifications

In order to fulfill "FR06 - The detection system around the detection model must notify its users that a contamination was detected", a simple cloud-based email service architecture was implemented using an AWS server with the architecture shown in Figure 17.

Figure 17 – Architecture developed for the email functionality of the system.

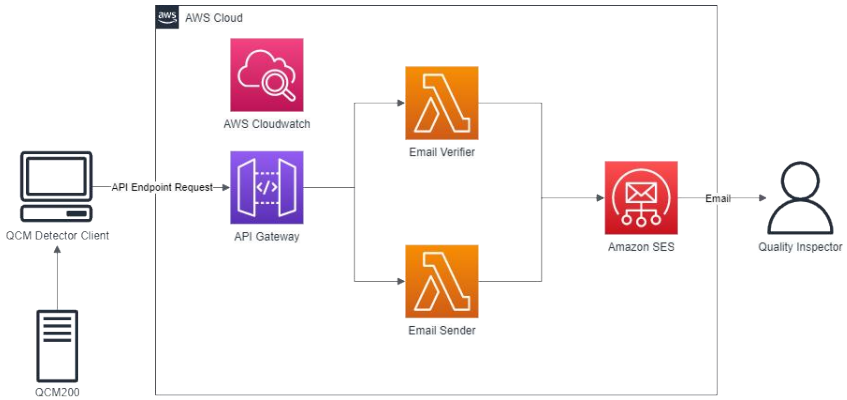

Source: Self authorship

In this architecture, the data is streamed from the QCM200 into a computer that has access to the internet, after a contamination has been detected, the system makes an API request to the AWS Api Gateway to get access into the programmed lambdda functions that are divided into two: (i) the Email Verifier and (ii) the Email Sender.

The (i) email verifier is responsible for sending a verification email in order to register the email in the AWS Simple Email Service (SES). Then, when the email has been verified, when a detection is made within the system's operation, the (ii) will receive a request with the detection information, such as time, severity and the destination email, as parameters for it to request the SES to send the appropriate email to the end user. All of these modules are monitored through a programmed AWS Cloudwatch module that will notify the system's administrator if unexpected behaviors in the system occur in order for appropriate action to be taken.

5.2.3 System Architecture

The overall architecture of the system was first introduced in Section 4.3, and it presented an MVC-style architecture. Using that model in mind, the architecture shown in Figure 18 was implemented in python using the QT GUI framework to implement the user interface.

Figure 18 – Architecture Diagram of the System implemented

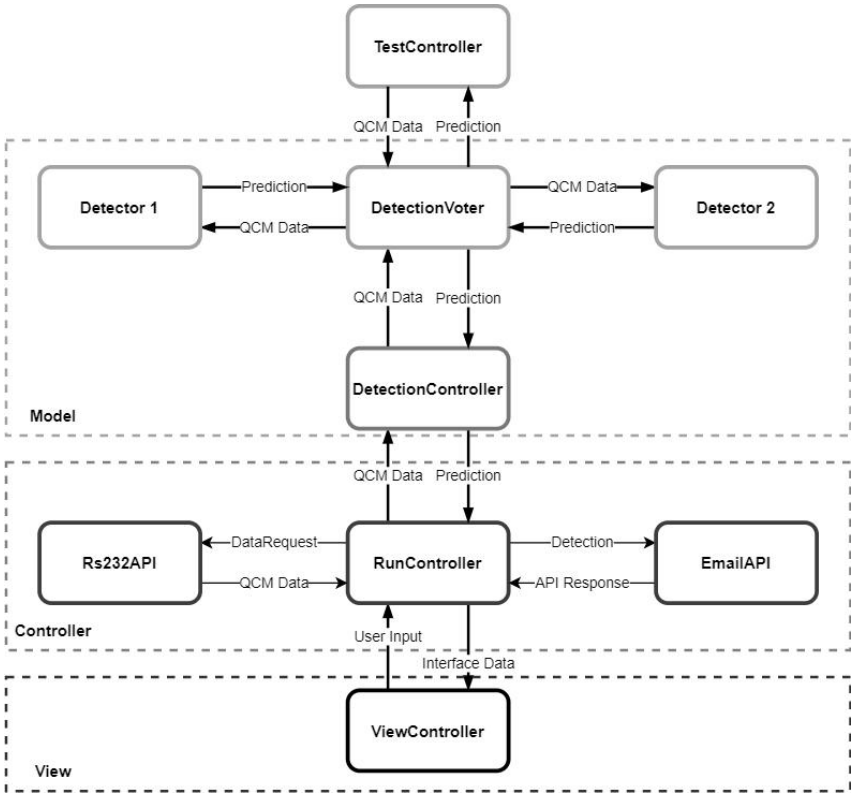

Source: Self authorship

In the implemented architecture, the **ViewController** is responsible for displaying the GUI to the user, handling the user's inputs into the system, and handling changes in the interface such as events of connection with the QCM, readouts from the QCM and others.

The **ViewController** and the **RunController** are very intimately connected, in the sense that the **RunController** is responsible for managing the internal run-state of the system, such as the state of the connections between the system and the QCM, the management of internal memory access with Mutex elements and the creation and management of parallel threads. This class is the one that controls the flow of the data that is being received from the QCM.

These two elements compose an element in the MVC architecture called the View-Controller element, where both the handling of the user's inputs and the displaying of information to the user are both handled by a single class or by a set of classes. This is done so that the handling of user information does not need to pass through a dedicated controller class to get to the model, being more adequate to smaller systems such as the one being implemented.

Further back in the system there is the **DetectionController** and the **DetectionVoter**. The **DetectionController** is responsible for keeping track of the detections that have been made, which detectors have made the detection and of sending the detections back to the **RunController**.

The **DetectionVoter**, as described in the previous section, is an intermediary class that takes the QCM data from the **DetectionController** and sends it to all of its detectors, receiving back their detections and voting whether or not there has been a detection and how severe that detection is based on the current and previous detections.

Lastly, the **test controller** was the class responsible for the implementation of the tests performed in Section 5.2.1.1, it acts as a simulated RunController and it records the detected contaminations in order to check which ones were correct or not.

5.2.4 RS232 Interface

The interface with the QCM is made through the RS232 interface it provides. Its functionality is based on commands that can be sent to the QCM or requests for information that can be provided. Some of the possible commands are shown in Figure 19 (STANFORD, 2004).

To implement the interface with it, within the system, there is a parallel worker thread that is responsible for asynchronously reading the interface with the QCM when requested to, to do so it needs to query the absolute resistance and frequency, wait for the QCM to return the required info, and return it to the RunController.

The query can done simply by sending either the "R"or "F"digits through the RS232 interface and waiting for a response from the RS232 bus. In order to treat edge cases of faulty connections, the request can timeout after 1 second without a response from the QCM, in case more than 10 timeouts happen in a row, the system will be disconnected from the QCM.

Figure 19 – Commands available for the QCM 200

F — **Query Absolute Frequency**

Query the Absolute Frequency.

Example

F<CR> Returns the Absolute Frequency in Hz.

G(?) — **Frequency Offset**

Set the Frequency Offset value or query the Relative Frequency.

Relative Frequency = Absolute Frequency – Frequency Offset

Example

G<CR> Set the Frequency Offset to the current Absolute Frequency.
G?<CR> Returns the Relative Frequency in Hz.

R — **Query Absolute Resistance**

Query the Absolute Resistance.

Example

R<CR> The Absolute Resistance is returned in Ohms.

S(?) — **Resistance Offset**

Set the Resistance Offset or query the Relative Resistance.

Relative Resistance= Absolute Resistance – Resistance Offset

Example

S<CR> Set the Resistance Offset to the current Absolute Resistance.
S?<CR> Returns the Resistance Offset in Ohms.

I — **Identification String**

Query the Identification String.

Example

I<CR> Returns a string similar to "QCM200 rev 1.04 s/n69001".

B — **Query Status**

Query the Status Byte. The value is returned as a decimal number from 0 to 255. The conditions for each bit are listed below.

Bit	Set by
0	New R value
1	New F value
2	Frequency Over Range
3	Frequency Under Range
4	Communication Error
5	unused
6	unused
7	unused

Example

B<CR> Returns the Status Byte in decimal format. Executing this

Source: Stanford Research (STANFORD, 2004)

5.2.5 Interface

In order to fulfill the FR05, the interface was developed using the python implementation of the QT front-end framework, it uses python code in order for it to render a 2D or 3D graphical user interfaces. It is implemented within the **ViewController** class described in Section 4.3.

The interface implemented contains the main user menu on the left-hand side, providing the buttons and input boxes for the input port, the output path, the email to be registered, along with assisting buttons to refresh the serial ports available, to select the output path of the data file, and to register the email. Along with these, there is a connect button for the system to start communicating through the RS232 port with the QCM200. The GUI can be seen with an example data streamed through it in Figure 20.

Figure 20 – The GUI developed for the project

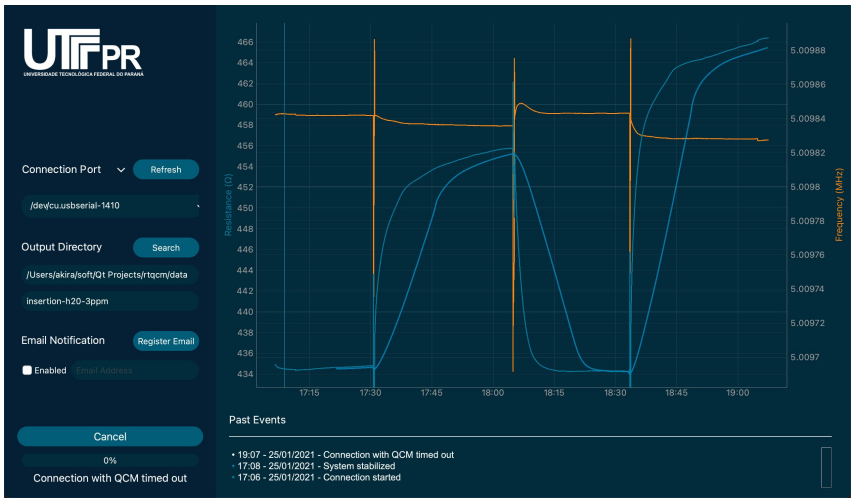

Source: Self authorship

6 Results

6.1 Measurement Phase

6.1.1 Preliminary results

Using the setup defined in Section 15, the preliminary experiment was to (i) insert the crystal in the water and examine its behavior, waiting for it to come to a stable state and (ii) to insert a high concentration of ammonia in order to determine its response to it.

The definition of a high concentration of ammonia was deemed to be of around $5mg/L$ of NH_4OH^-, based on the related works shown in Section 2 this is a concentration well above what is expected for the sensors to respond.

Figure 21 – Preliminary experiment of $5mg/L$

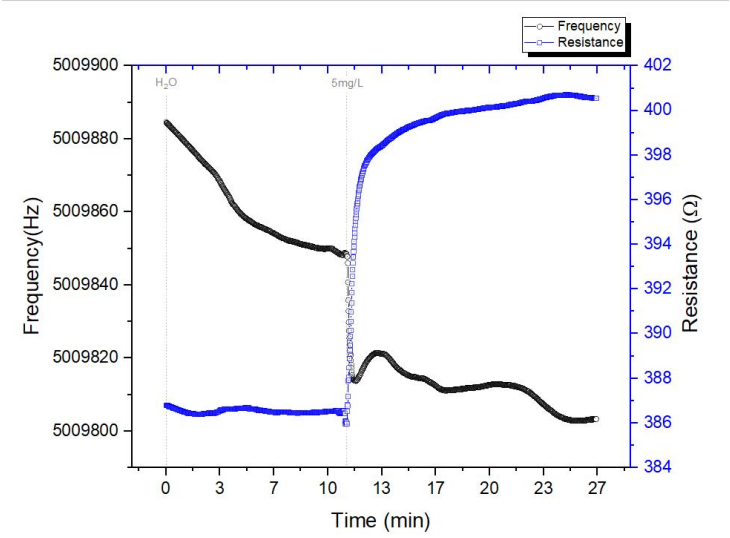

Source: Self authorship

The results of the experiment are shown in Figure 21, from which, we can clearly tell that there was a significant reaction when the sensor was exposed to $5mg/L$ of ammonium hydroxide. The interactions that can be seen are: (i) An increase of 24Ω in the crystal's motional resistance and (ii) A decrease in $78Hz$ in the crystal's resonant frequency.

Effect (ii) of a decrease in the crystal's resonant frequency, according to equation 3.1 could be attributed to an adherence of ammonia particles to the sensor through the interaction between ammonia and the dangling bonds of the PANI/rGO composite, making the crystal have more mass on its surface, decreasing its resonant frequency.

Effect (i) on the other hand is harder to describe analytically, it is the increase of the motional resistance of the crystal/film interface, one possible explanation is the change of PANI

being in its Emeraldine Salt form into its Emeraldine Base form, which has a more viscous nature, raising the resistance the crystal has of displacing it on its surface.

To confirm these findings, the same experiment was done on $10mg/L$ of ammonium hydroxide and the results can be seen in Figure 22, in which we can clearly see the same effects taking place.

Figure 22 – Preliminary experiment of $10mg/L$

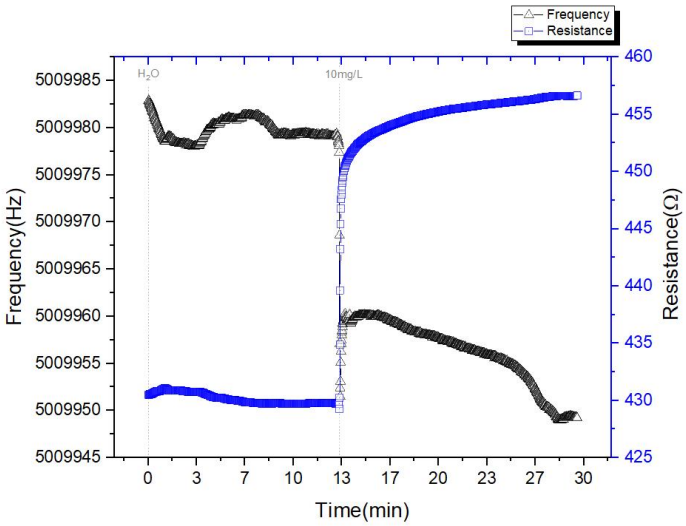

Source: Self authorship

$$\begin{aligned}
\Delta R_{5mg/L} &= \frac{R_f - R_0}{R_0} \\
\Delta R_{5mg/L} &= \frac{400.63 - 386.51}{386.51} = 0.0365 \\
\Delta R_{5mg/L} &= 3.65\%
\end{aligned}$$

$$\begin{aligned}
\Delta R_{10mg/L} &= \frac{R_f - R_0}{R_0} \\
\Delta R_{10mg/L} &= \frac{456.64 - 429.74}{429.74} = 0.0626 \\
\Delta R_{10mg/L} &= 6.26\%
\end{aligned}$$

Further analyzing the resistance in the results of Figures 21 and 22, it can be seen that the percentage difference in response to $5mg/L$ was of 3.65% and the one for $10mg/L$ was of 6.26% so an increase of almost double in the response, which means the sensor has a consistent response to increasing concentrations of ammonia in water.

6.1.2 Calibration curve

To further study the behavior of the sensor, a series of experiments with increasingly high concentrations of ammonia must be done in succession, this aids in the comprehension of

how low the detections can be made, how good the sensor is in comparison to other state of the art electrochemical sensors.

To do this, the contamination experiment that was done in Section 6.1.1 for $5mg/L$ and $10mg/L$ were repeated for the concentrations of $1mg/L$, $3mg/L$, $5mg/L$, $10mg/L$, $30mg/L$, $50mg/L$, $100mg/L$ and $200mg/L$.

Figure 23 – Calibration Curve experiment results

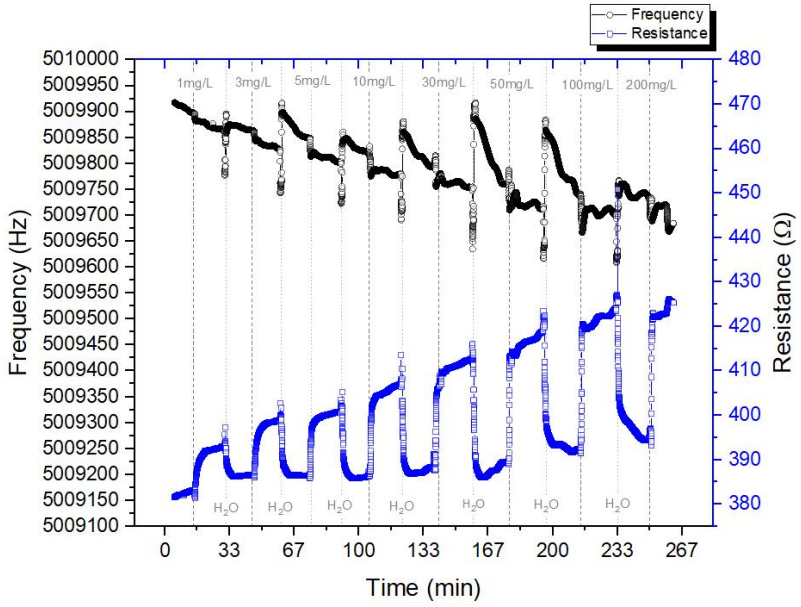

Source: Self authorship

From the data, is it noticeable how noisy the resonant frequency is, this could be explained by its faster nature of it being related to the mass adsorbed on the surface of the crystal, as opposed to the slower interaction between Emeraldine Salt and ammonia molecules that result in the change in its motional resistance. To better analyze the results, the changes in resistance were plotted in relation to the added ammonia to the water. The results are shown in Figure 24 in a semi-log scale.

These data were collected using only the resistance measurements because the frequency data was too noisy to be able to be used as steady state measurements before and after the contaminants were introduced.

Figure 24 – Calibration Curve response fit results

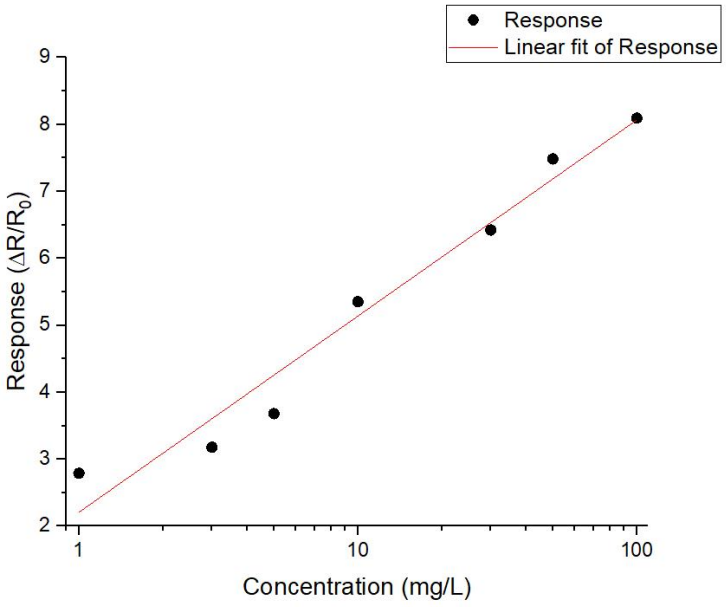

Source: Self authorship

The fit in Figure 24 has an R^2 value of 0.9633 and a pearson's R score of 0.98148, from which can be seen that the sensor has a range beyond the limits of $1mg/L$ and $100mg/L$, and from the data, the limit of detection can be calculated according to (ANDERSON, 1989) by the following equation:

$$LOD_{y/x} = 3\frac{\sigma_{y/x}}{S_{y/x}}$$

Applying this equation to the linear fit from Figure 24, an LOD of $458.29775\mu g/L$ of Ammonium Hydroxide was found. To compare with regulatory requirements, the concentration of ammonium hydroxide must be converted into total ammonia nitrogen (TAN), the main metric used by regulatory organizations (HUFF et al., 2013). To do that, the LOD must be multiplied by the ratio between the molecular weight of nitrogen and the molecular weight of ammonium hydroxide, doing that yields an LOD_{TAN} of $LOD_{TAN} = 183.20\mu g/L$ of TAN.

Doing a similar procedure to discover the LOD in M $(mols/L)$, it can be found that the $LOD_{mol} = LOD/35.04 = 13.0792\mu M$, being comparable to the other electrochemical sensors shown in Section 2. Comparing this composite to a film of PANI by itself, and performing the same procedures as those used to produce the graph in Figure 24 on the QCM coated only with PANI, the results shown in Figure 25 was achieved.

Figure 25 – Comparison of PANI/rGO and PANI on a QCM crystal

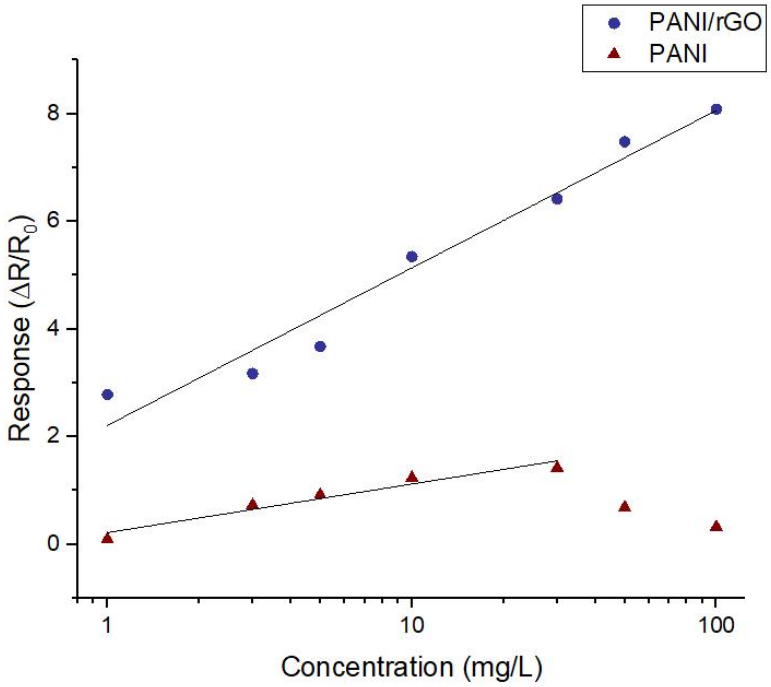

Source: Self authorship

In Figure 25, it can be seen that the the response achieve with only PANI on the QCM was inferior to that achieved with the PANI/rGO composite. With the response of the PANI film at $30mg/L$ being inferior to that of the PANI/rGO film at $1mg/L$, and with a visible amount of drop-off in response of the PANI film in concentrations above that, possibly indicating its saturation point being lower than that of the PANI/rGO film. Therefore, it can be seen that there is a significant improvement from the addition of the rGO film to the composite.

Another aspect that can be seen from the data in Figure 24 is that the response $\Delta R/R_0$ starts at around a 2% variation of the initial resistance level. This was used in Section 5.2 in order to tune the thresholds of the Exponential Forecast and Mean Deviation detectors.

6.1.3 Building the dataset

The procedures brought up in Section 5.1.3 were followed and a series of experiments were done in progressively bigger concentrations of ammonium hydroxide, starting from the concentration of $0.5mg/L$ of it. One new addition to the tests is the presence of longer experiments that would leave the sensor for over 8 hours submerged to see if temperature and measurement drifts would be an issue. A sample of the results of those experiments can be seen in the figures presented in Figure 26

Figure 26 – Samples from the dataset built from the experiments performed

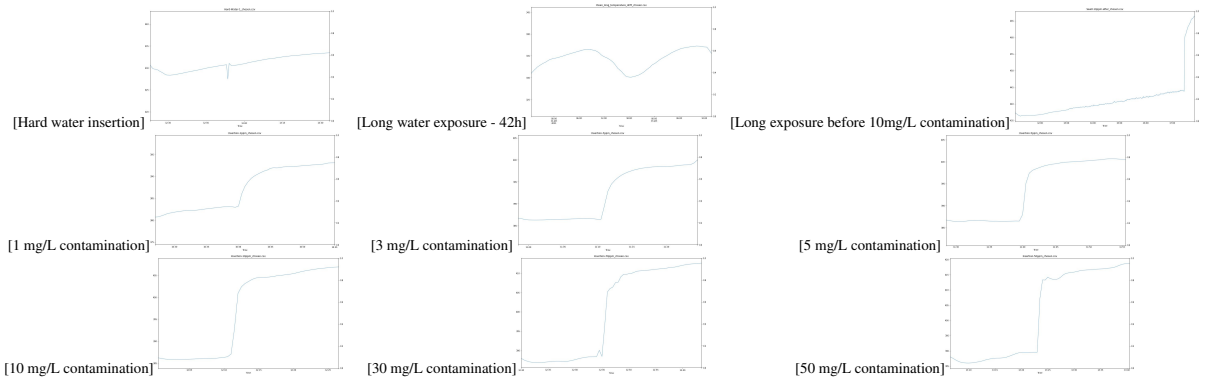

Source: Self authorship

6.2 Development Phase

6.2.1 Algorithms analysis

In Section 5.2, the algorithms relevant to this project were implemented around the **DetectionVoter**, seen in Figure 18. To evaluate them, all of the tests performed with the QCM sensor were compiled and the correct times for contamination detection were tabulated, and, along with the **TestController** class, used for evaluating each algorithm and how many false positives and true positives it had. The results obtained are shown in Table 2.

Table 2 – Results of each algorithm

Algorithm	**False Positives**	**True Positives**	**Recall**
Isolation Forest	694	264	38.0%
OCSVM	20	20	50.0%
Exponential Forecast	0	20	100.0%
Mean Deviation	0	30	100.0%

With these results, it can be seen that the simpler methods have far outperformed the commonly used anomaly detection methods, this might be because of the simpler nature of the data from the QCM, being more adequate to be used by less complex models that were calibrated with real experiment data, something that is not easily embedded in models such as OCSVM and Isolation Forests.

Examples of the detections made by each of the algorithms are shown in Figures 28, 29, 27, and 30. Figures 28, 29 and 27 show that in experiments without noise or measurement drift, all algorithms were able to perform well, having their detections withi a valid detection zone.

Figure 27 – Detections made by each algorithm in a 5mg/L contamination of $NH4OH$

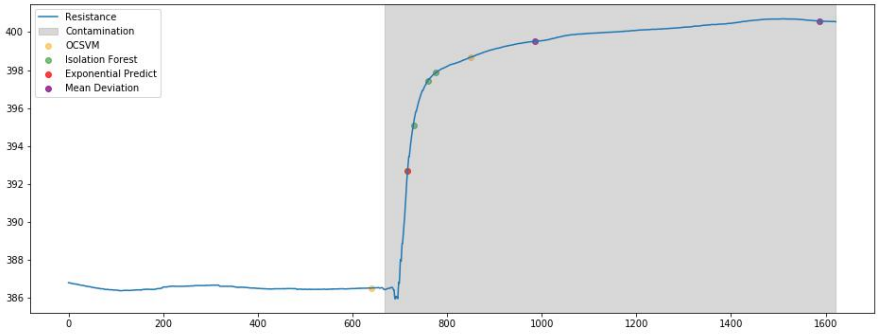

Source: Self authorship

Figure 28 – Detections made by each algorithm in a 10mg/L contamination of $NH4OH$

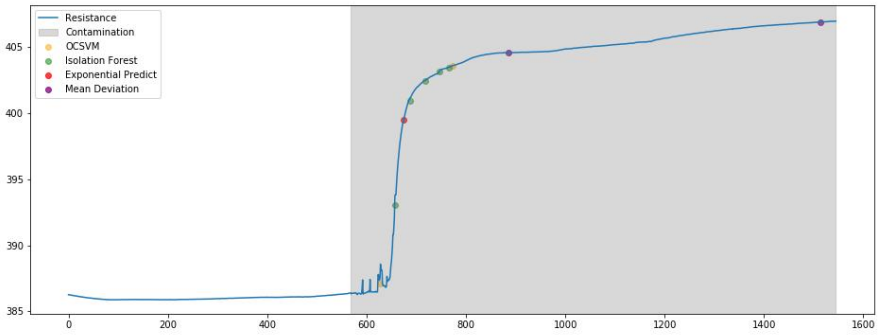

Source: Self authorship

Figure 29 – Detections made by each algorithm in a 10mg/L contamination of $NH4OH$

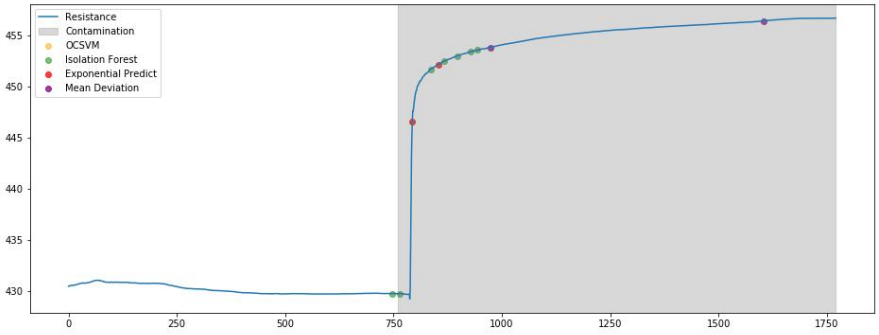

Source: Self authorship

However, when there is considerable drift caused by temperature changes or any kind of deviation from the norm, such as is the case in the experiment shown in Figure 30 in which the sensor was left overnight and then was exposed to the contamination. In this experiment, both

the OCSVM and Isolation Forest Algorithms detected several anomalies due to the drift caused by the change in temperature throughout the night, while the Mean Deviation and Exponential Forecast algorithms detected the contamination correctly.

Figure 30 – Detections made by each algorithm in a long water water exposure experiment, the contamination is of 10mg/L of $NH4OH$

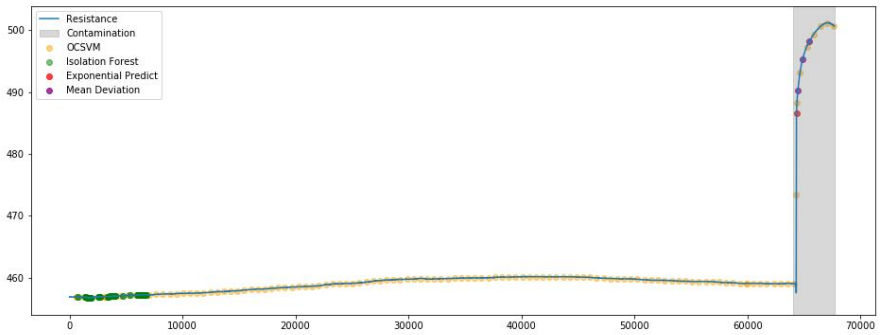

Source: Self authorship

There is an argument to be made that OCSVM and Isolation Forest would outperform the Exponential forecast if subjected to hyper-parameter tuning, but considering the computational cost of both methods in lieu of the performance achieved with the Exponential Forecast and Mean Deviation Techniques, they were discarded for the rest of the project and only the Exponential Forecast and Mean Deviation detectors were used.

There were only 2 cases where the mean deviation and exponential forecast systems gave a false negative prediction to an experiment but in both situations, the contamination was under the control measure stipulated in this project, these experiments are shown in Figures 31 and 32. Meaning that a combination of both the exponential forecast and mean deviation algorithms could still be used as an appropriate detector along with the mean deviation detector. With this, the main component of FR07 was achieved from the performance of both the Exponential Forecast and Mean Deviation algorithms.

Figure 31 – Detections made by each algorithm in a the contamination of 0.5mg/L of $NH4OH$

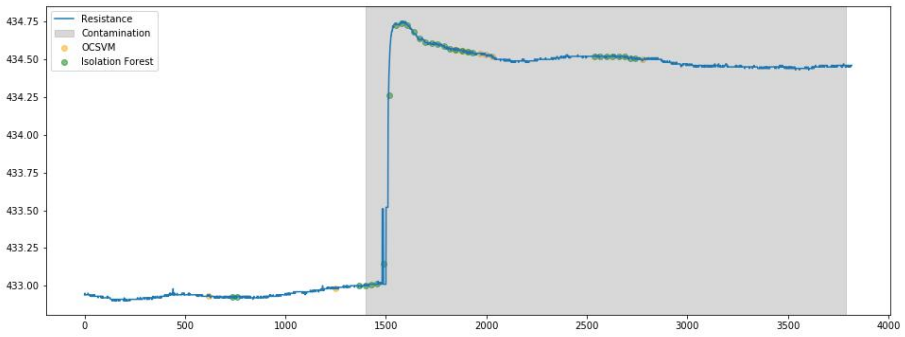

Source: Self authorship

Figure 32 – Detections made by each algorithm in a contamination of 1mg/L of $NH4OH$

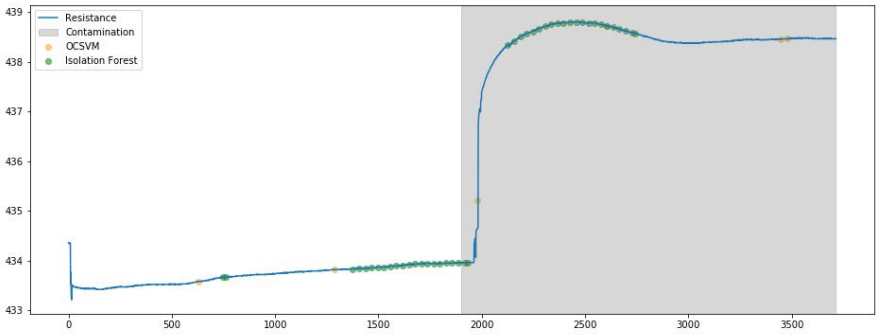

Source: Self authorship

6.2.2 Final system assembly

By joining together all of the components as described in Figure 18. The system was assembled and it was tested with a contamination of $5mg/L$ of Ammonium Hydroxide and the result in the GUI is shown in Figure 33

Figure 33 – Final interface with a contamination of $5mg/L$ of ammonium hydroxide, with the detected contaminations visible from the graph

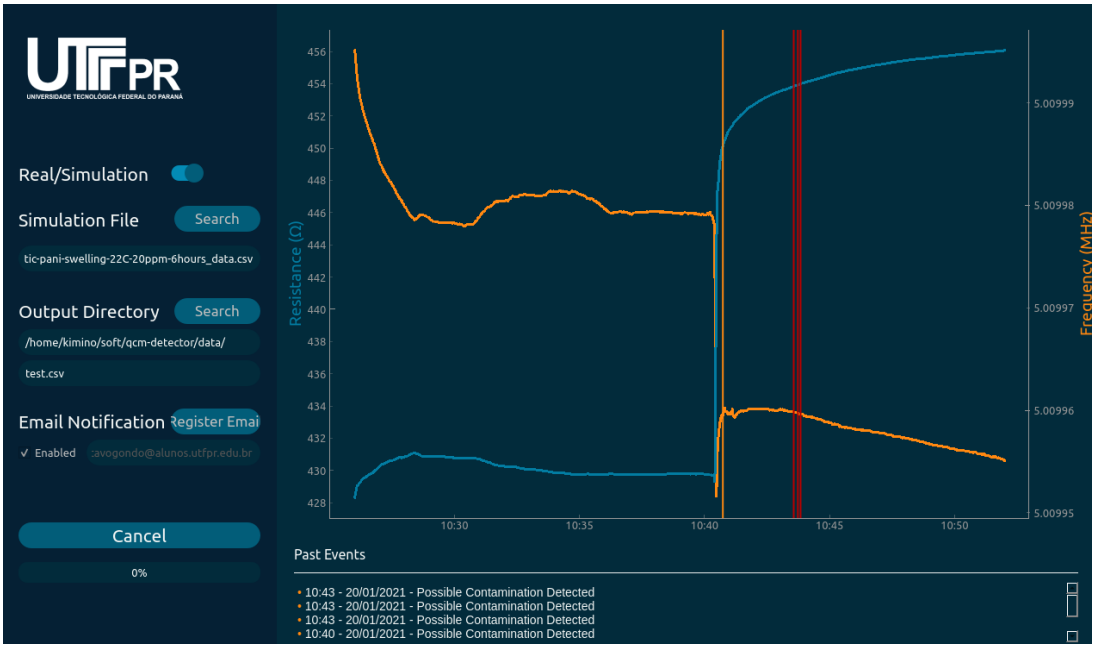

Source: Self authorship

The resulting contaminations led to the system sending an email to the email registered on the text field on the left side of the GUI, and the email received is shown in Figure 34

Figure 34 – Resulting email from the detected contamination

Source: Self authorship

7 Final Considerations

7.1 Final Considerations

In summary, through an analysis of the different capabilities of the Quartz Crystal Microbalance and PANI/rGO sensor system, a reproducible experimental setup was developed for testing of water under various conditions. Along with that, considering the consequences of both acute an long-term exposure to ammonia in different concentrations, and analyzing the current state-of-the-art polyaniline ammonia sensors, a control measure was defined in order to validate the system.

After that, a comparative test with different detection models was performed on the data collected from several ammonia contaminations on the test setup and it was chosen that the simple Mean-deviation and the Exponential Forecast algorithms had the best overall performances and were chosen in order to be components of an ensemble-like contamination detection model. This model was developed using python along with an auxiliary graphical user interface in order for it to be used in a real world setting. As an added feature, an email notification system was developed using an AWS cloud-based infrastructure, so that remote personnel would be able to be notified in case a contamination was detected and for the relevant data to be logged in their emails.

With that, the model was tested and the GUI and email functionalities were tested. All of the tests were correctly assessed by the ensemble system, therefore passing the validation criteria imposed previously.

7.2 Future works

Due to the scope of this work, there are several possibilities of future developments for this work, a few of which are listed below.

- The execution of repeatability and selectivity tests of the PANI/rGO films on QCM crystals, in order to assert how reproducible and selective these results are; as well as how durable the sensor is;
- An expansion of the GUI functionalities, expanding the email notifications functionality into an email-login system that could lock the interface with a password;
- An auxiliary setting to tune how sensitive the system is to any contaminations;

- The development of a packaged, embedded solution that would contain the system developed without the bulk needed by the QCM200, enabling the system to be either handheld or easily portable;
- Utilizing more than one QCM crystal in tandem, in order to classify different contaminants using more sophisticated classifier, such as KNN, Principal component analysis and SVM.

References

AHMAD, S. et al. Unsupervised real-time anomaly detection for streaming data. *Neurocomputing*, v. 262, p. 134–147, 2017. ISSN 0925-2312. Disponível em: <https://www.sciencedirect.com/science/article/pii/S0925231217309864>. Cited on page 40.

ANDERSON, D. J. Determination of the lower limit of detection. *Clinical chemistry*, Oxford University Press, v. 35, n. 10, p. 2152–2153, 1989. Cited 2 times on pages 36 and 50.

ARUGULA, M. A.; SIMONIAN, A. L. Chapter 10 - biosensors for detection of genetically modified organisms in food and feed. In: WATSON, R. R.; PREEDY, V. R. (Ed.). *Genetically Modified Organisms in Food*. San Diego: Academic Press, 2016. p. 97–110. ISBN 978-0-12-802259-7. Disponível em: <https://www.sciencedirect.com/science/article/pii/B9780128022597000105>. Cited 2 times on pages 23 and 24.

CHEN, Q. et al. Qcm-d study of nanoparticle interactions. *Advances in colloid and interface science*, Elsevier, v. 233, p. 94–114, 2016. Cited on page 21.

CHEN, Z. et al. Electrochemical analysis of conducting reduced graphene oxide/polyaniline/polyvinyl alcohol nanofibers as supercapacitor electrodes. *Journal of Materials Science: Materials in Electronics*, Springer Nature, v. 31, n. 8, p. 5958–5965, apr 2020. ISSN 09574522. Disponível em: <http://10.0.3.239/s10854-020-03204-1>. Cited 2 times on pages 18 and 20.

CROWLEY, K. et al. An aqueous ammonia sensor based on an inkjet-printed polyaniline nanoparticle-modified electrode. *The Analyst*, v. 133, p. 391–9, 04 2008. Cited on page 18.

ESLAMI, M. R.; ALIZADEH, N. Ultrasensitive and selective qcm sensor for detection of trace amounts of nitroexplosive vapors in ambient air based on polypyrrole—bromophenol blue nanostructure. *Sensors and Actuators B: Chemical*, v. 278, p. 55–63, 2019. ISSN 0925-4005. Disponível em: <https://www.sciencedirect.com/science/article/pii/S0925400518316800>. Cited on page 12.

FANG, F. F.; SUNG, J. H.; CHOI, H. J. Shear stress and dielectric characteristics of polyaniline/tio2 composite-based electrorheological fluid. *Journal of Macromolecular Science, Part B*, Taylor $ Francis, v. 45, n. 5, p. 923–932, 2006. Disponível em: <https://doi.org/10-.1080/00222340600865119>. Cited on page 18.

GAO, R. et al. Research and improvement of isolation forest in detection of local anomaly points. In: IOP PUBLISHING. *Journal of Physics: Conference Series*. [S.l.], 2019. v. 1237, n. 5, p. 052023. Cited on page 26.

HADANO, F. S. et al. Improved Sensitivity. 2021. Cited 5 times on pages 12, 18, 19, 20, and 35.

HU, Y. et al. The surface chemical composition effect of a polyacrylic acid/polyvinyl alcohol nanofiber/quartz crystal microbalance sensor on ammonia sensing behavior. *RSC advances*, Royal Society of Chemistry, v. 8, n. 16, p. 8747–8754, 2018. Cited on page 17.

HUANG, X. et al. Reduced graphene oxide–polyaniline hybrid: Preparation, characterization and its applications for ammonia gas sensing. *J. Mater. Chem.*, The Royal Society of Chemistry, v. 22, p. 22488–22495, 2012. Disponível em: <http://dx.doi.org/10.1039/C2JM34340A>. Cited on page 20.

HUANG, Y. et al. A novel all-solid-state ammonium electrode with polyaniline and copolymer of aniline/2,5-dimethoxyaniline as transducers. *Journal of Electroanalytical Chemistry*, v. 741, p. 87–92, 2015. ISSN 1572-6657. Disponível em: <https://www-.sciencedirect.com/science/article/pii/S1572665714006079>. Cited 2 times on pages 16 and 36.

HUFF, L. et al. Aquatic life ambient water quality criteria for ammonia-freshwater. *US Environmental Protection Agency*, v. 10, 2013. Cited 3 times on pages 12, 36, and 50.

JOHANNSMANN, D. Studies of viscoelasticity with the qcm. In: ____. [S.l.: s.n.], 2007. v. 5, p. 49–109. ISBN 978-3-540-36567-9. Cited 2 times on pages 23 and 24.

KAN, Y. et al. An all-solid-state ammonium ion-selective electrode based on polyaniline as transducer and poly (o-phenylenediamine) as sensitive membrane. *Int. J. Electrochem. Sci*, v. 11, p. 9928–9940, 2016. Cited 2 times on pages 16 and 36.

KNOBELOCH, L. et al. in Environmental Medicine. n. November 1999, p. 675–678, 2000. Cited on page 36.

LAVIN, A.; AHMAD, S. Evaluating real-time anomaly detection algorithms – the numenta anomaly benchmark. In: *2015 IEEE 14th International Conference on Machine Learning and Applications (ICMLA)*. [S.l.: s.n.], 2015. p. 38–44. Cited on page 40.

LEE, C. T.; WANG, Y. S. High-performance room temperature NH3 gas sensors based on polyaniline-reduced graphene oxide nanocomposite sensitive membrane. *Journal of Alloys and Compounds*, Elsevier Ltd, v. 789, p. 693–696, jun 2019. ISSN 09258388. Cited on page 20.

LI, D. et al. Detection methods of ammonia nitrogen in water: A review. *TrAC - Trends in Analytical Chemistry*, Elsevier Ltd, v. 127, p. 115890, 2020. ISSN 18793142. Disponível em: <https://doi.org/10.1016/j.trac.2020.115890>. Cited on page 12.

LI, Q.; GU, Y.; JIA, J. Classification of multiple chinese liquors by means of a qcm-based e-nose and mds-svm classifier. *Sensors*, v. 17, n. 2, 2017. ISSN 1424-8220. Disponível em: <https://www.mdpi.com/1424-8220/17/2/272>. Cited on page 17.

LIU, F. T.; TING, K. M.; ZHOU, Z.-H. Isolation forest. In: IEEE. *2008 eighth ieee international conference on data mining*. [S.l.], 2008. p. 413–422. Cited 2 times on pages 24 and 25.

LIU, G.; ZHANG, G. *QCM-D studies on polymer behavior at interfaces*. [S.l.]: Springer, 2013. Cited 4 times on pages 12, 20, 21, and 22.

MAITY, D.; MANOHARAN, M.; KUMAR, R. T. R. Development of the pani/mwcnt nanocomposite-based fluorescent sensor for selective detection of aqueous ammonia. *ACS Omega*, v. 5, n. 15, p. 8414–8422, 2020. Disponível em: <https://doi.org/10.1021/acsomega-.9b02885>. Cited on page 18.

MAJUMDAR, D.; BASKEY, M.; SAHA, S. K. Epitaxial Growth of Crystalline Polyaniline on Reduced Graphene Oxide. *Macromolecular Rapid Communications*, John Wiley & Sons, Ltd, v. 32, n. 16, p. 1277–1283, aug 2011. ISSN 1022-1336. Disponível em: <https://doi.org/10.1002/marc.201100292>. Cited on page 20.

Mohamad Ahad, I. Z. et al. Polyaniline (pani) optical sensor in chloroform detection. *Sensors and Actuators B: Chemical*, v. 261, p. 97–105, 2018. ISSN 0925-4005. Disponível em: <https://www.sciencedirect.com/science/article/pii/S0925400518300820>. Cited on page 18.

OH, J. et al. Ultrasensitive and Selective Organic FET-type Nonenzymatic Dopamine Sensor Based on Platinum Nanoparticles-Decorated Reduced Graphene Oxide. *ACS Applied Materials & Interfaces*, American Chemical Society, v. 9, n. 45, p. 39526–39533, nov 2017. ISSN 1944-8244. Disponível em: <https://doi.org/10.1021/acsami.7b15093>. Cited on page 18.

OKUR, S. et al. Identification of mint scents using a qcm based e-nose. *Chemosensors*, Multidisciplinary Digital Publishing Institute, v. 9, n. 2, p. 31, 2021. Cited on page 17.

PEDREGOSA, F. et al. Scikit-learn: Machine learning in Python. *Journal of Machine Learning Research*, v. 12, p. 2825–2830, 2011. Cited 2 times on pages 26 and 27.

RAY, S. C. Application and Uses of Graphene Oxide and Reduced Graphene Oxide. *Applications of Graphene and Graphene-Oxide Based Nanomaterials*, n. May, p. 39–55, 2015. Cited on page 19.

ROTO, R. et al. Enhanced sensitivity and selectivity of ammonia sensing by qcm modified with boric acid-doped pvac nanofiber. *Sensors and Actuators A: Physical*, v. 304, p. 111902, 2020. ISSN 0924-4247. Disponível em: <https://www.sciencedirect.com/science/article/pii-/S0924424719321636>. Cited on page 16.

SHAKTAWAT, V.; SAXENA, N.; SHARMA, K. Study of the structure and mechanical properties of pure and doped polyaniline. *Phase Transitions*, Taylor & Francis, v. 84, n. 3, p. 215–224, 2011. Disponível em: <https://doi.org/10.1080/01411594.2010.534655>. Cited on page 18.

SONG, S. et al. Optimization of 3d surfaces of dextran with different molecule weights for real-time detection of biomolecular interactions by a qcm biosensor. *Polymers*, v. 9, n. 9, 2017. ISSN 2073-4360. Disponível em: <https://www.mdpi.com/2073-4360/9/9/409>. Cited on page 12.

STANFORD, R. S. Qcm200 quartz crystal microbalance digital controller service manual. 2004. Cited 5 times on pages 22, 23, 37, 44, and 45.

SU, X. et al. A wireless electrode-free qcm-d in a multi-resonance mode for volatile organic compounds discrimination. *Sensors and Actuators A: Physical*, v. 305, p. 111938, 2020. ISSN 0924-4247. Disponível em: <https://www.sciencedirect.com/science/article/pii-/S0924424719315717>. Cited on page 17.

SVOBODOVÁ, Z. *Water quality and fish health*. [S.l.]: Food & Agriculture Org., 1993. Cited on page 36.

VAUGHAN, R.; O'SULLIVAN, C.; GUILBAULT, G. Development of a quartz crystal microbalance (qcm) immunosensor for the detection of listeria monocytogenes. *Enzyme and Microbial Technology*, Elsevier, v. 29, n. 10, p. 635–638, 2001. Cited on page 21.

VIRJI, S. et al. Polyaniline nanofiber gas sensors: Examination of response mechanisms. *Nano Letters*, v. 4, n. 3, p. 491–496, 2004. Disponível em: <https://doi.org/10.1021/nl035122e>. Cited on page 18.

WAN, C.; JIAO, Y.; LI, J. Flexible, highly conductive, and free-standing reduced graphene oxide/polypyrrole/cellulose hybrid papers for supercapacitor electrodes. *J. Mater. Chem. A*, The Royal Society of Chemistry, v. 5, p. 3819–3831, 2017. Disponível em: <http://dx.doi.org/10.1039/C6TA04844G>. Cited on page 20.

WANG, A. et al. Reduced graphene oxide covalently functionalized with polyaniline for efficient optical nonlinearities at 532 and 1064nm. *Dyes and Pigments*, v. 160, p. 344–352, 2019. ISSN 0143-7208. Disponível em: <https://www.sciencedirect.com/science/article/pii-/S0143720818314220>. Cited on page 20.

WU, K. et al. The fabrication of all solid-state ammonium ion selective electrodes used in aquaculture. In: *2017 IEEE SENSORS*. [S.l.: s.n.], 2017. p. 1–3. Cited 2 times on pages 16 and 36.

WU, Z. et al. Enhanced sensitivity of ammonia sensor using graphene/polyaniline nanocomposite. *Sensors and Actuators B: Chemical*, Elsevier, v. 178, p. 485–493, 2013. Cited on page 18.

YILMAZ, E. et al. Whole cell imprinting based escherichia coli sensors: A study for spr and qcm. *Sensors and Actuators B: Chemical*, Elsevier, v. 209, p. 714–721, 2015. Cited on page 21.